Opto-Electronic Science

CN 51-1800/O4 ISSN 2097-0382 (Print) ISSN 2097-4000 (Online)

Enrichment strategies in surface-enhanced Raman scattering: theoretical insights and optical design for enhanced light-matter interaction

Zhiyang Pei, Chang Ji, Mingrui Shao, Yang Wu, Xiaofei Zhao, Baoyuan Man, Zhen Li, Jing Yu and Chao Zhang

Citation: Pei ZY, Ji C, Shao MR, et al. Enrichment strategies in surface-enhanced Raman scattering: theoretical insights and optical design for enhanced light-matter interaction. *Opto-Electron Sci* **4**, 250015 (2025).

https://doi.org/10.29026/oes.2025.250015

Received: 12 May 2025; Accepted: 14 July 2025; Published online: 18 September 2025

Related articles

Opto-Electronic Science

Review

December 2025, Vol. 4, No. 12

DOI: 10.29026/oes.2025.250015 CSTR: 32246.14.oes.2025.250015

Enrichment strategies in surface-enhanced Raman scattering: theoretical insights and optical design for enhanced light-matter interaction

Zhiyang Pei, Chang Ji, Mingrui Shao, Yang Wu, Xiaofei Zhao, Baoyuan Man, Zhen Li*, Jing Yu* and Chao Zhang*

Surface-enhanced Raman scattering (SERS) is a powerful molecular fingerprinting technique widely applied across physical chemistry, environmental monitoring, and public safety. While hotspot engineering has driven significant advances, a critical limitation persists: the reliable detection of analytes lacking affinity for plasmonic surfaces remains challenging. Despite extensive reviews on SERS substrates and hotspots (>300 in recent years), none systematically address analyte manipulation as a complementary paradigm for overcoming this universal detection barrier. This review uniquely synthesizes the rapidly evolving field of analyte enrichment strategies—categorized as chemical, physical, and macroscopic force field approaches—and demonstrates their integration with engineered hotspots as a multifaceted solution. We highlight how this synergy achieves unprecedented sensitivity enhancements (10^4–10^{15} fold), unattainable through hotspot engineering alone. Finally, we emphasize the current challenges in this research area and propose new research directions aimed at developing efficient SERS designs that are critical for real-world applications.

Keywords: surface enhanced Raman scattering; analyte enrichment; chemical modification; physical concentration; macroscopic force field restriction

Pei ZY, Ji C, Shao MR et al. Enrichment strategies in surface-enhanced Raman scattering: theoretical insights and optical design for enhanced light-matter interaction. *Opto-Electron Sci* **4**, 250015 (2025).

Introduction

Surface enhanced Raman scattering (SERS) is a non-invasive spectroscopic technique that utilizes unique molecular vibrational fingerprints to identify and quantify analytes down to ultra-trace levels[1–14]. The dominant mechanism underlying the enhancement in SERS can be categorized into physical enhancement[15–17] and chemical enhancement[3,18]. Physical enhancement arises from localized surface plasmon resonance (LSPR), which significantly amplifies the Raman signals by the noble metal nanostructures. Chemical enhancement, on the other hand, stems from a weaker response initiated by charge transfer between the analyte and the substrate. Typically, these two mechanisms do not operate independently but are coupled, working synergistically to influence the overall enhancement effect of Raman scattering[19–23]. Theoretically, the intensity of the Raman signal conforms to the following formula[9]:

School of Physics and Electronics, Shandong Normal University, Jinan 250014, China.

*Correspondence: Z Li, E-mail: lizhen19910528@163.com; J Yu, E-mail: yujing1608@126.com; C Zhang, E-mail: czsdnu@126.com

Received: 12 May 2025; Accepted: 14 July 2025; Published online: 18 September 2025

$$\begin{aligned} I(\omega_P) &= AI_0(\gamma_0,\omega)|\alpha(\omega_R,\omega)|^2 \times G(\gamma_0) \\ &= AI_0(\gamma_0,\omega)|\alpha(\omega_R,\omega)|^2 \\ &\quad \times |E(\gamma_0,\omega)|^4/|E_0(\gamma_0,\omega)|^4, \end{aligned} \tag{1}$$

here, A represents the collection efficiency of Raman signal, I_0 stands for the intensity of the incident light, α indicates the Raman scattering cross-section of the molecule, and G denotes the enhancement factor. Verified by extensive experiments and calculations, the Raman scattering process can be regarded as a complex interaction between incident light, substrate and molecules. Consequently, the enhancement of Raman signals can be approached from three major perspectives: 1) Enhancing incident light intensity and signal collection efficiency: through the construction of micro-nano hollow or porous structures, this method aims to improve the utilization of incident light by the substrate. For instance, in 2018, Professor Bin Ren's group introduced a novel gapless three-dimensional SERS substrate featuring a unique hybrid plasmonic optical cavity (HPOC) structure, fabricated by using tunable holographic lithography combined with gold deposition techniques. This HPOC structure can capture and match specific wavelengths of excitation light by adjusting the physical scale of the optical cavity, thereby significantly enhancing the strength of the SERS signal[24]. 2) Amplifying local electromagnetic field intensity to improve enhancement factor: this strategy primarily leverages the physical enhancement mechanism, which is predominant in SERS. The process entails the optimization of the characteristics of hotspots within metallic nanostructures (known as "hotspot engineering"). Parameters such as the surface morphology of noble metal nanoparticles, adjacent gaps, and compositional methods are meticulously adjusted to maximize the intensity of local electromagnetic field. For instance, in 2021, Barveen NR et al. utilized photochemical methods to synthesize gold nanostars on flexible PMMA substrates. The strong electric field excitation effect at the tips of these gold nanostars led to the formation of numerous hotspots, resulting in exceptional detection sensitivity and signal reproducibility[25]. 3) Increasing the Raman scattering cross-section: this approach targets molecules with low Raman cross-sections that lack interaction with plasmonic surfaces. It generally involves coupling reactions to modify the chemical structure, thereby expanding the molecular Raman cross-section and generating resonance Raman scattering (RRS). A notable study using a plasma liquid marble platform demonstrated this concept. Initially, non-resonant environmental toxin Bisphenol A (BPA), which possesses an electronic transition wavelength of 280 nm and no affinity for silver, did not exhibit significant SERS features initially. However, after coupling BPA with an aryl azo cation, the resultant-colored molecule exhibited an absorption peak at 476 nm, achieving a SERS limit of detection of 10 attomoles. This detection limit is 50000 times lower than the safety limit for BPA and 10^7 times more sensitive than UV-visible absorption spectroscopy detection[26].

Over the past five decades, SERS technology has made significant strides and found applications in diverse fields such as food safety[27], atmospheric, environmental monitoring[28] and early disease diagnosis[29–34]. Despite these advancements, the industrialization of SERS still faces several challenges[35]. A primary obstacle is the insufficient coupling between hotspots and target molecules, which include volatile organic compounds (VOCs)[36–38], foodborne pathogenic bacteria[39–41], heavy metal ions[42,43], and other analytes. These molecules often present difficulties in obtaining clear and reproducible Raman signals, thereby limiting the practical utility of SERS in practical scenarios. To address these challenges, researchers have sought to modulate the distribution patterns of hotspots to achieve more efficient and uniform enhancement. Traditional static surface Raman spectroscopy structures typically feature narrow and non-tunable plasmonic gaps, which limit their ability to detect analytes of varying sizes. Consequently, efforts have been directed toward developing more adaptable hotspot configurations that can enhance detection sensitivity and specificity for a broader range of molecular targets. Professors YungDoug Suh and Dai-Sik Kim proposed an adaptive gap-tunable SERS substrate, utilizing flexible gold nano-gaps and adaptive optical control to selectively enhance and modulate different plasmonic vibration modes. By designing the gap width, the tunability of plasmon resonance reaches up to 1200 cm^{-1}, primarily attributed to the excellent mechanical bending properties of the polyethylene terephthalate substrate. This further confirms that tunable plasmon resonance can selectively enhance different Raman spectral regions of molecules[44]. Furthermore, to achieve more uniformly distributed hotspots, large-area, arrayed nanostructures have been widely adopted. For instance: Shin-Hyun Kim and colleagues utilized optical methods to create multi-dimensional metallic structures with three different

periodicities[45], Ji and co-workers employed a thermal-assisted method to synthesize micron-scale TiO_2 ink for the large-scale fabrication of SERS-active semiconductor microsphere arrays[46], Kuniharu Ijiro's team arranged gold nanotriangles (AuNTs) on the surface of thermoresponsive hydrogels, fabricating arrays of gold nanotriangles on gel surfaces (AuTAGs)[47]. These designed arrayed SERS substrates not only exhibit excellent optical response properties but also enable the synergistic effects of multiple resonance modes through the modulation of parameters such as size, morphology, and periodicity. This further enhances the uniformity and diversity of hotspot distribution, leading to superior detection performance and reliability.

In addition to modulating the distribution of hotspots, developing innovative strategies to establish effective associations between hotspots and target molecules is key to advancing SERS technology. Researchers have observed that when trace analytes aggregate near hotspot regions, the intensity and stability of their Raman signals are significantly enhanced. This deliberate manipulation to concentrate analytes within hotspot regions is known as enrichment technology. In recent years, the integration of SERS detection with enrichment technologies has revealed unique and complementary advantages. Firstly, these combined approaches ensure that analytes are more effectively exposed to hotspot regions, thereby enhancing detection stability and sensitivity, leading to faster and more accurate detection outcomes. Secondly, the integration broadens the application scope of SERS, enabling it to meet a wider range of testing requirements. It also opens new avenues for the development and optimization of analytical platforms, ultimately advancing the practical utility and versatility of SERS technology.

Currently reported SERS enrichment strategies can be categorized into three types: chemical enrichment strategies, physical enrichment strategies, and macroscopic force field enrichment strategies. In chemical enrichment strategies, the surfaces of SERS substrates are typically functionalized with a variety of specific functional groups. These functional groups facilitate the integration of target molecules through chemical reactions, aiding in their selective screening and enrichment within complex liquid or gas phases, thereby achieving specific molecular recognition. However, practical applications reveal several challenges: 1) Non-specific binding: non-target compounds may also adhere to the substrate due to electrostatic interactions, hydrophobic effects, or other intermolecular forces, leading to increased background noise and potential false-positive results. 2) Functional group instability: under certain conditions, the modified functional groups may degrade or detach from the substrate, particularly when exposed to extreme pH levels, temperature fluctuations, or specific solvents. Such instability not only diminishes the efficiency of enrichment but can also result in false-negative outcomes. Physical enrichment strategies for SERS involve designing substrates that possess intrinsic physical enrichment or screening capabilities. These methods leverage the physical properties of the substrate, such as shape, size, charge, and wettability, to confine target molecules within hotspot regions. As a result, this approach is label-free and exhibits minimal dependence on the chemical properties of the analytes. However, it generally suffers from poor selectivity, low efficiency, a tendency to cause sample loss, and limited applicability across different types of samples. Macroscopic force field enrichment strategies involve utilizing principles of mechanical equilibrium to separate and concentrate target analytes, which are subsequently detected using SERS substrates. This approach simplifies the preparation process for SERS substrates by focusing on pre-treating the analytes to achieve lossless enrichment under specific conditions. However, this method primarily depends on the physical properties of the analytes and faces several challenges due to its reliance on separation equipment: 1) Non-specific separation: when target substances share similar physical characteristics with non-target substances, mechanical enrichment methods may fail to effectively distinguish between them, leading to non-specific enrichment and contamination. 2) Operational complexity and high costs: techniques such as high-speed centrifugation and high-pressure filtration require sophisticated equipment and precise operation. This not only increases operational complexity but also drives up costs, making these methods less accessible and more resource-intensive. 3) Sample losses: during mechanical enrichment, samples can be lost through adsorption on container walls, clogging of filter media, or sedimentation at the bottom of centrifuge tubes. Such losses reduce recovery rates and compromise the accuracy of analytical results. 4) Limited processing capacity: the processing capacity of mechanical enrichment methods is often constrained by equipment limitations and operational parameters. For large-scale processing or continuous flow systems, additional design and optimization efforts may be necessary

to meet throughput requirements.

Over the past decade, enrichment techniques have advanced significantly, demonstrating substantial potential across a wide array of applications. Despite this progress, there remains a relative paucity of comprehensive reviews dedicated specifically to enrichment strategies for SERS detection. Consequently, there is an urgent need for a new review that encapsulates these advancements while exploring future directions. In this review, we systematically examine the design methodologies of enrichment techniques developed for SERS over the past decade, highlighting their strengths and limitations. We delve into innovative strategies employed to enhance analyte concentration and specificity, as well as the challenges faced in practical applications. Additionally, we explore other promising enrichment methods that can be synergistically combined with SERS to broaden its utility and effectiveness. By providing a thorough analysis of current practices and emerging trends, it is hoped that this review will foster deeper research into enrichment SERS technologies, stimulate interdisciplinary collaboration, and offer multiple pathways for accelerating the development and industrialization of SERS.

Why introduce enrichment in SERS

As discussed above, SERS exhibits tremendous potential in practical applications due to its ultra-sensitive trace analysis capabilities. Particularly, by employing micro and nanotechnologies to engineer the shape, size, or gap distance of metal nanostructures—referred to as "hotspot engineering"[48–54], which is possible to modulate the local electromagnetic field strength associated with plasmons more reliably. However, probe molecules that are generally employed to characterize the activity of SERS substrates exhibit a particular affinity for hotspots. This pronounced adsorption effect facilitates the collection of Raman signals, thereby serving as an effective benchmark for substrate performance. Nevertheless, this approach evidently fails to represent the analytes encountered in practical applications. Consequently, a critical question arises: "how can these highly active SERS platforms be made effective for detecting molecules that have no or only weak affinity for plasmons?"

To address the challenge of detecting low-affinity molecules with SERS, it is necessary to enhance their interaction with SERS substrates. This can be achieved by introducing functional materials during substrate preparation[55–63] or via analyte enrichment during the detection process[64]. The former approach involves enhancing or extending the substrate's performance during preparation by incorporating additional functional materials, thereby improving the binding capability and detection sensitivity for target molecules. For instance, combining metal nanoparticles with specific functional nanomaterials (graphene[4,59,60,65,66], carbon nanotubes[67–70], quantum dots[71–73], and emerging 2D plasmonic materials such as TMDs, heterostructures etc.), can significantly improve the substrate's specific surface area, conductivity, and photoelectric response properties. These enhancements lead to better adsorption of target analytes and more efficient detection. Additionally, using self-assembled monolayer technology to form ordered molecular layers on metal surfaces can provide specific binding sites that enhance interactions with target molecules, further boosting detection sensitivity and specificity. However, most material composite processes currently require multi-step synthesis and strict control over parameters such as temperature, pressure, pH, and reaction time during preparation, therefore resulting in higher costs, poorer reproducibility, and more complex operations. Moreover, the functional tuning may lack flexibility, making it challenging to meet the diverse needs of different application scenarios.

Compared to introducing functional materials, analyte enrichment has garnered widespread attention due to its operational simplicity and intuitive mechanism. This strategy employs a variety of methods to confine or localize analytes on SERS-active surfaces, thereby significantly enhancing the sensitivity and reproducibility of SERS signals. It is particularly effective for molecules that lack specific affinity for plasmonic surfaces and possess low Raman cross-sections. By concentrating these analytes, the enrichment process effectively removes most non-target substances, reducing background noise and improving detection selectivity. Notably, enrichment techniques are not only diverse, well-established, and highly adaptable across various application fields but also have the potential to boost trace detection capabilities and enable the precise capture of target molecules in complex environments, thus broadening the practical utility of SERS and paving the way for large-scale industrial applications.

Reported SERS enrichment strategies

In this section, we will examine analyte enrichment techniques in SERS, with the central objective of increasing

the concentration of analytes in proximity to plasmonic surfaces through various strategies. We will provide a comprehensive overview of three mature SERS enrichment strategies (illustrated in Fig. 1): 1) chemical enrichment strategies[74–79], 2) physical enrichment strategies[80–93], 3) macro force field enrichment strategie[94–104], and offer a detailed analysis of the strengths, limitations, and application scenarios for each strategy.

Chemical enrichment strategy

Chemical enrichment strategies leverage specific chemical or biochemical interactions —including covalent bonding, coordination chemistry (e.g., metal-ligand binding), hydrogen bonding, ionic interactions, bio affinity binding (e.g., antibody-antigen, aptamer-target, lectin-carbohydrate), molecular imprinting, and host-guest chemistry—to selectively capture and concentrate target analytes onto the SERS-active substrate[105–107]. This approach is universally applicable across diverse analyte classes, ranging from small molecules, ions, and gases to proteins, nucleic acids, viruses, and whole bacterial cells. The underlying principle hinges on the modification or functionalization of the surface of SERS-active substrates with functional groups that can specifically bind to the target analytes. This approach ensures the provision of more reliable detection conditions for molecules that exhibit stable chemical characteristics, weak adsorption capabilities, or poor interaction with hotspots.

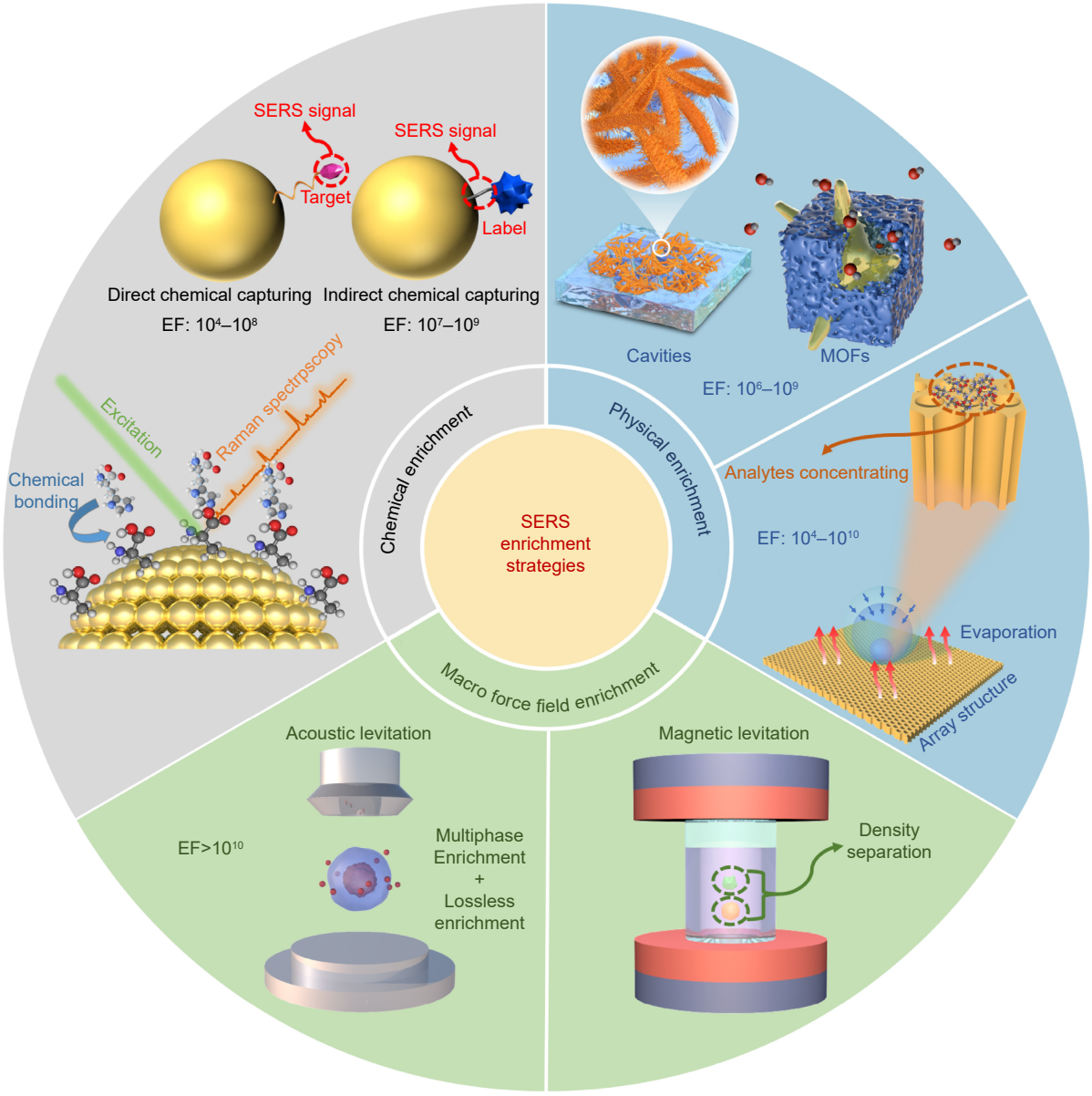

Fig. 1 | Overview of SERS enrichment strategies.

Depending on the origin of the Raman signal, chemical enrichment strategies can be classified into two main categories: direct chemical enrichment strategies[74,75,78] and indirect chemical enrichment strategies[76,77,79], as illustrated in Fig. 2.

Direct chemical enrichment strategies

Direct chemical enrichment strategies entail the specific capture of target molecules on the surface of noble metal nanoparticles via chemical reactions between functional groups on the substrate and the analytes (Fig. 3(a)). This detection method elucidates the fingerprint vibrational information of the captured analytes' relevant chemical bonds directly, and has been applied to detect pollutants generated in industrial production, such as phthalate esters (PAEs), which are widely used plasticizers that can easily permeate into the natural environment under the influence of pH and temperature changes, causing sudden pollution of water, soil, and even the atmosphere. In the detection of PAEs, polydopamine (PDA) serves as a linker to integrate molecularly imprinted polymers (MIPs) with gold nanoparticles[74]. The resulting SERS-active AuNPs/PDA-MIP coating serves as a modifier to functionalize screen-printed electrodes, which are then used for the selective enrichment and detection of PAEs and relevant analogues (Fig. 3(b)).

Furthermore, direct chemical enrichment strategies have been employed in the sensing of biomacromolecules, including multiplex analysis of microRNA. As shown in Fig. 3(c), a microreactor utilizes individual microbeads coated with a protonated layer[75]. On this protonated layer, S9.6 antibodies serve as a universal module for binding different sequences of DNA/miRNA duplexes. Concurrently, each set of gold nanoparticle signal amplifiers is labeled with Raman encoded molecules and DNA probes to specifically capture target RNA on the plasmonic layer, thereby significantly amplifying the SERS signal. This method concentrates miRNA-induced SERS signals within the tiny surface area of a single microbead, markedly enhancing the sensitivity of SERS-based detection. Additionally, the SERS signal can be further enhanced by a pre-coated plasmonic gold nanoparticle layer.

In addition to the chemical capture and specific detection of single-category analytes, direct chemical enrichment strategies have been employed in the development of high-throughput SERS platforms. These platforms enable the rapid capture and identification of multiple analytes by functionalizing distinct regions of the substrate surface with diverse functional groups. For instance, Ling et al. developed a SERS taste sensor capable of high-throughput, specific recognition of five wine flavor

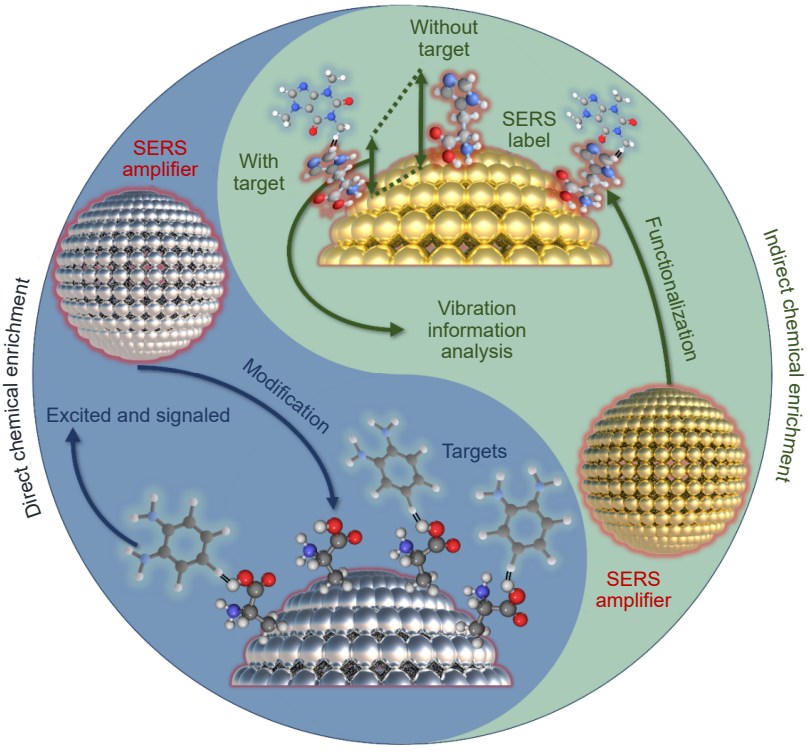

Fig. 2 | Overview of SERS-chemical enrichment strategy.

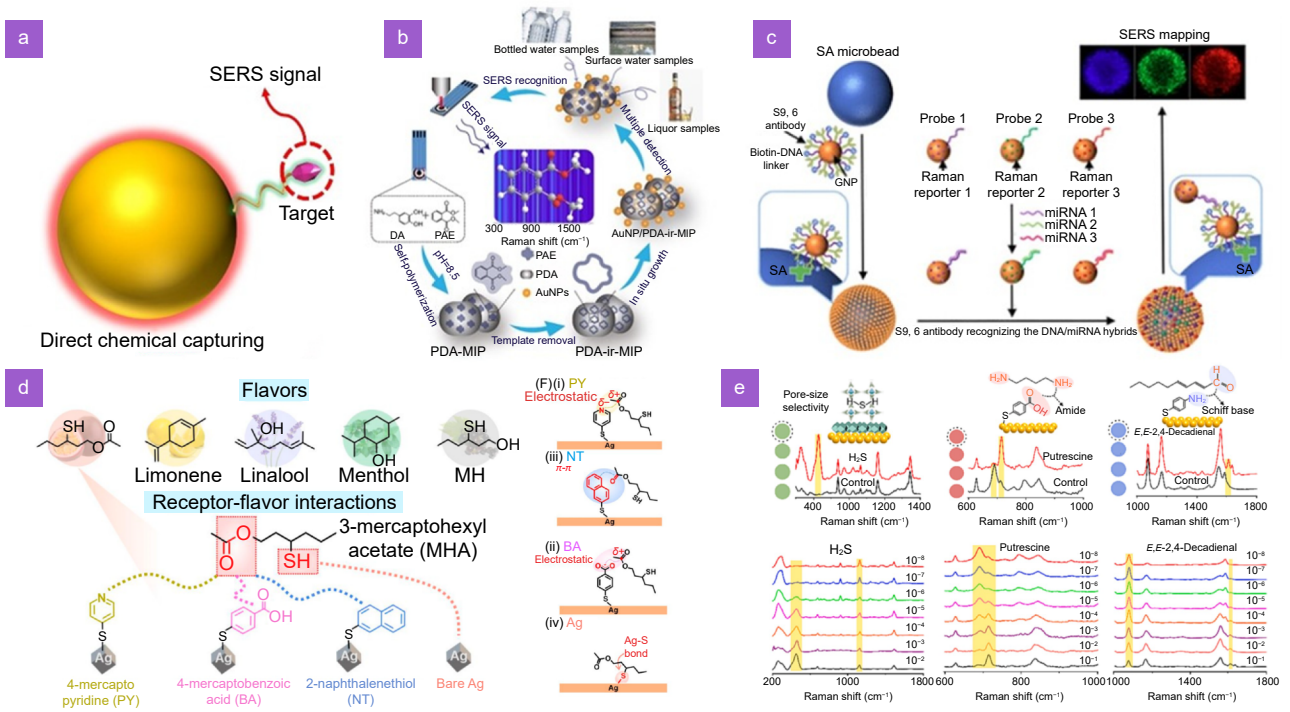

Fig. 3 | (**a**) Working schematics of SERS-direct chemical enrichment strategies. (**b**) Molecularly imprinted polymers linked to gold nanoparticles using polydopamine as a linker for selective enrichment and detection of plasticizer PAEs. (**c**) Schematic illustration of multiplexed miRNA assay on a single plasmonic microbead. (**d**) Specific capture of different odor molecules by introducing four receptors for specific capture and high-throughput SERS recognition. (**e**) Selective capture of VOCs such as bacterial metabolites, hydrogen sulfide, acetaldehyde, biogenic amines, and other VOCs and generation of unique SERS spectral images by integrating the functionalized coating's on the surface of the array. Figure reproduced with permission from: (b) ref.[74], Copyright 2020 Elsevier; (c) ref.[75], Copyright 2021 American Chemical Society; (d) ref.[78], Copyright 2021 American Chemical Society; (e) ref.[108], Copyright 2024 Elsevier.

molecules: higher fatty alcohols like menthol, terpenes such as linalool and limonene, and sulfur-containing compounds including 3-mercaptohexyl acetate and 3-mercaptohexanol[78] (Fig. 3(d)). These flavor molecules typically exhibit weak Raman scattering cross-sections, making them difficult to detect even with advanced chromatographic techniques. By introducing four different receptors, the prepared SERS substrate can specifically capture different odor molecules through chemical reactions. By strategically combining all receptor-flavor SERS spectra, a comprehensive "SERS hyperspectrum" was constructed for predictive analysis using chemometrics. The same strategy has also been applied to multi-dimensional identification and quantification of various foodborne VOCs. As illustrated in Fig. 3(e), by integrating functionalized coatings on array surfaces, the substrates can selectively capture and generate unique SERS spectral signatures for a variety of compounds, including bacterial metabolites, hydrogen sulfide, acetaldehyde, biogenic amines, and other VOCs[108]. The multi-dimensional signal output significantly enriches the complexity of VOC fingerprints, thereby markedly enhancing the sensitivity, reliability, and accuracy of freshness assessments and predictive analyses in real food odor evaluations.

Indirect chemical enrichment strategies

Indirect chemical enrichment strategies are typically used to detect molecules with weak vibrational fingerprints or inactive Raman vibrations, such as gases, biomolecules, and ions. Unlike direct detection, this approach involves modifying the substrate surface with molecules that not only specifically bind to the target analytes but also generate strong Raman signals, these molecules are referred to as Raman tags. The success of this strategy primarily relies on observable changes in SERS vibration intensity or energy caused by alterations in molecular configuration upon conjugation of the Raman tags with the analytes. Therefore, in indirect SERS detection, researchers exploit changes in the vibrational modes of the Raman tags to detect the presence of analytes, rather than relying on the inherent molecular

fingerprints of the analytes themselves (Fig. 4(a)). For example, Tian et al. reported a novel SERS nanosensor, 4-acetamidophenylsulfonyl azide-functionalized gold nanoparticles (AuNPs/4-AA) for the detection of endogenous H_2S in live cells[77]. Detection is realized by monitoring the SERS spectral changes of AuNPs/4-AA upon the reaction of H_2S with 4-AA on the gold nanoparticle surface. The prepared AuNPs/4-AA exhibit a rapid response to H_2S within 1 min and demonstrate a sensitivity of 0.1 mmol.

In the biological domain, to achieve highly sensitive detection of pathogens, Gu et al. developed a biocompatible platform for indirect chemical capture. As illustrated in Fig. 4(b), this biosensor uses wheat germ agglutinin-modified raspberry-like Fe_3O_4@Au magnetic nanoparticles as capturing agents to enrich target pathogens. Additionally, it utilizes co-freezing aptamer/5,5'-dithiobis-(2-nitrobenzoic acid)/gold nanoparticles tags as the signal source[110]. This method achieved successful detection of the *IS6110* gene from Mycobacterium tuberculosis, demonstrating a sensitivity lower than 500 fM, with a linear response ranging from 1 pM to 10 nM. Additionally, the detection exhibited specificity towards the *IS6110* gene.

Similarly, for the multiplex immunoassay diagnosis of various bacteria, Wang et al. developed a multiplex SERS-immunochromatographic platform. This platform employs thin-film magnetic tags based on graphene oxide, designated as GFe-DAu-D/M, which are capable of efficiently capturing and detecting multiple bacterial species from complex samples (Fig. 4(c))[76]. The two-dimensional GFe-DAu-D/M tag is fabricated by sequentially assembling a layer of small Fe_3O_4 nanoparticles (NPs) and two layers of 30 nm AuNPs (with an inner 0.5 nm nanogap) on a single-layer graphene oxide nanosheet. The tag is further co-modified with 4-mercaptophenylboronic acid (MPBA) and 5,5'-dithiobis. This innovative design not only facilitates the rapid

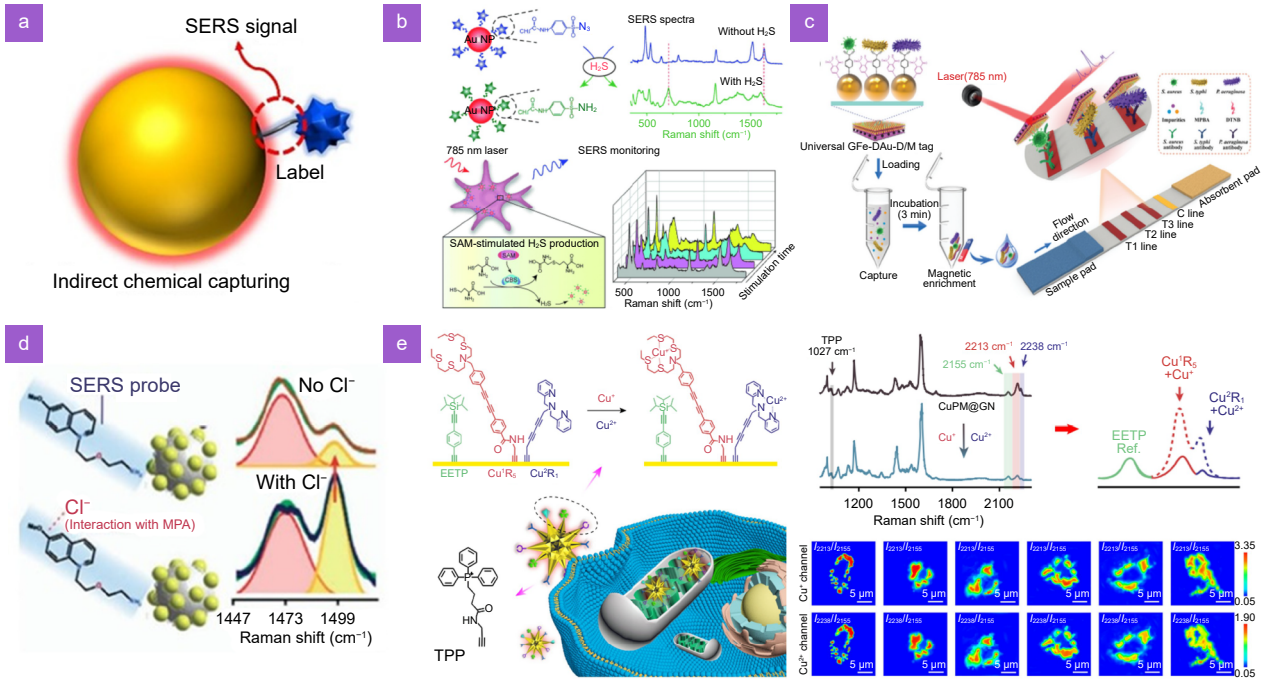

Fig. 4 | (**a**) Working schematics of SERS-indirect chemical enrichment strategies. (**b**) Schematic illustration of the principle for capturing endogenous H_2S in live cells using 4-acetamidobenzenesulfonyl azide-functionalized gold nanoparticles (AuNPs/4-AA) and achieving highly sensitive sensing of H_2S through changes in the Raman spectroscopic vibrations of 4-AA. (**c**) GFe-DAu-D/M-ICA SERS substrates used for multiplex detection of Staphylococcus aureus, Salmonella typhi, and Pseudomonas aeruginosa. (**d**) A chloroion-sensitive organic fluorophore is grafted onto a silver surface deposited on micrometer-sized silica beads. The π-π interaction between chloride ions and the fluorophore's aromatic ring causes geometric and electronic changes in the latter, increasing the intensity ratio of ring stretching modes at 1497 and 1472 cm^{-1} with rising Cl^- concentration, enabling picomolar-level detection of Cl^-. (**e**) A series of molecules containing different spacer lengths of ethylene derivatives were designed and synthesized as Raman reporters, and alkyne-tagged SERS probes were created for highly selective and sensitive determination of Cu^+ and Cu^{2+}, along with SERS imaging of both ions. Figure reproduced with permission from: (b) ref.[77], Copyright 2015 John Welly and Sons; (c) ref.[76], Copyright 2024 John Welly and Sons; (d) ref.[109], Copyright 2011 American Chemical Society; (e) ref.[79], Copyright 2024 Springer Nature.

enrichment of multiple bacterial species via MPBA but also integrates specific antibodies for the quantitative analysis of target bacteria. By leveraging magnetic enrichment and signal amplification from dense multilayer hotspots, it significantly reduces background interference in practical applications. More importantly, this technology can simultaneously diagnose three significant pathogens —Staphylococcus aureus, Pseudomonas aeruginosa, and Salmonella typhimurium (detection limit as low as 10 cells per milliliter). Furthermore, it has demonstrated excellent performance in the detection of real urinary tract infection samples, offering broad prospects for highly sensitive monitoring of bacterial infections or contamination.

Additionally, indirect chemical enrichment methods are also employed for detecting Raman-invisible ions such as chloride and copper ions. For instance, in the detection of chloride ions (Cl^-), a Cl^- sensitive organic fluorophore is attached to a silver surface deposited on silica microbeads[109]. The interaction between Cl^- and the aromatic ring of the fluorophore through π-π stacking causes geometric and electronic changes. As the concentration of Cl^- increases, it enhances the intensity ratio of the ring-stretching modes at 1497 and 1472 cm^{-1} (Fig. 4(d)). This non-destructive quantitative detection method achieves picomolar sensitivity, which is 10^3 to 10^6 times better than conventional destructive Cl^- detection methods such as ion chromatography and atomic absorption/emission spectroscopy. In a separation example for the detection of copper ions, Liu et al. designed and synthesized a series of molecules containing various diacetylene derivatives as Raman reporters, creating alkyne-labeled SERS probes with high selectivity and sensitivity for detecting Cu^+ and Cu^{2+}. The developed SERS probes generate well-separated, distinguishable Raman fingerprint peaks in the cellular silent region and possess an inherent correction function, allowing for accurate quantification of Cu^+ and Cu^{2+}. Due to the assembly of the probes with the designed Au–C≡C groups, they exhibit long-term stability and demonstrate high temporal-spatial resolution for real-time imaging and simultaneous quantification of mitochondrial Cu^+ and Cu^{2+}. Using this powerful tool, it is possible to observe and monitor toxic stress responses caused by Cu^+ and Cu^{2+} in real time (Fig. 4(e))[79].

In summary, both direct and indirect chemical enrichment strategies enhance the molecular selectivity and enrichment capability of SERS substrates by chemically modifying the surface of noble metals. However, this approach also presents several challenges: 1) Chemical modifications may introduce signal interference, potentially compromising detection accuracy. 2) The interaction between analytes and the modified substrate surface may be time-consuming and necessitates stringent reaction conditions. 3) Chemical reactions may generate byproducts that compete with target analytes for adsorption sites, thereby affecting enrichment efficiency. Therefore, it is crucial to explore and develop more convenient, accurate, and broadly applicable enrichment strategies to overcome these limitations.

Physical enrichment strategies

In addition to modulating the chemical properties of the substrate, physically confining target molecules by exploiting morphological diversity is also a promising approach. Compared to chemical enrichment strategy, this strategy requires no labeling, less or not dependent on the chemical characteristics of the analytes, thereby introducing virtually no sources of signal interference, which is crucial for molecular detection, especially in liquid and gas phases.

Herein, we will examine two well-established physical enrichment strategies, classified by their structural types and application scenarios as illustrated in Fig. 5: 1) structure-based enrichment strategies[83,85,86,88–91,111–113], 2) wettability-related enrichment strategies[80–82,84,87,93].

Structure-based enrichment strategies

It has been demonstrated that SERS substrates with specialized morphologies enable precise control over the behavior of both gas-phase and liquid-phase analytes, facilitating their adsorption or confinement. These substrates can often be integrated with SERS hotspot engineering to concentrate target molecules within hotspot regions, achieving dual focusing of both the analytes and the electromagnetic fields. This approach significantly enhances the sensitivity of trace SERS detection. To date, two types of substrates have been extensively studied: 1) cavity-structured substrates[24,86,90–91,114–116], 2) metal-organic framework (MOF) and porous nanocage substrates[36,83,85,88–89,111–113,117], as illustrated in Fig. 6(a).

As a classic model, cavity structures are widely utilized in the preparation of SERS substrates due to their special resonant cavity effects and ability to confine analytes. Especially when modified with noble metal nanostructures, these substrates exhibit a large specific surface

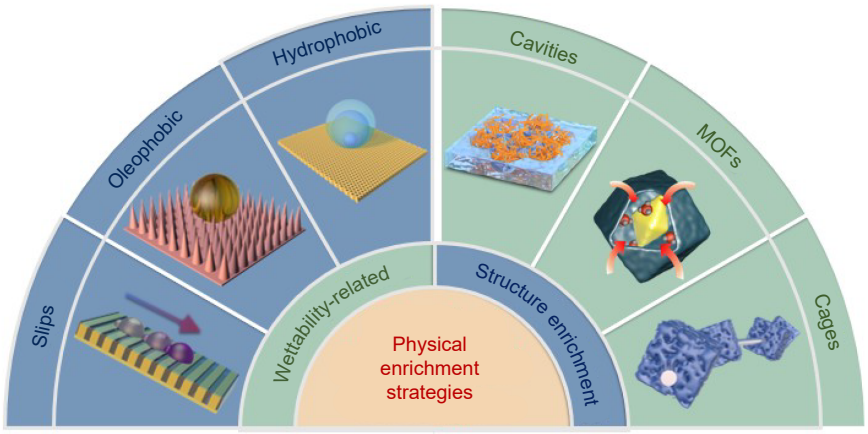

Fig. 5 | Overview of SERS-physical enrichment strategies.

area and three-dimensionally distributed hotspots, which effectively enhance the interaction between the SERS active regions and analytes, promoting molecular enrichment and signal amplification. Currently, the predominant cavity-structured enrichment can be primarily categorized into two types: passive enrichment and active enrichment. For instance, Yu et al. developed a particle-MoS_2 coated cavity structure composed of AAO/MoS_2/Ag, designed for the sensitive detection of water pollutants ranging from angstrom to hundreds of nanometers in size, including mercury ions (Hg^{2+}), 4-aminobenzenethiol, and polystyrene nanoplastics (100, 200, and 300 nm). As illustrated in Fig. 6(b), the inverted conical cavities of AAO act as ideal containers that capture and confine particles within the cavity[86]. Owing to the curvature of the cavity, the analytes inside are fully enveloped by Ag nanoislands on the side walls, enabling local hotspots to interact effectively with the plastic contaminants. This design exemplifies a typical passive enrichment, which relies on the free diffusion of

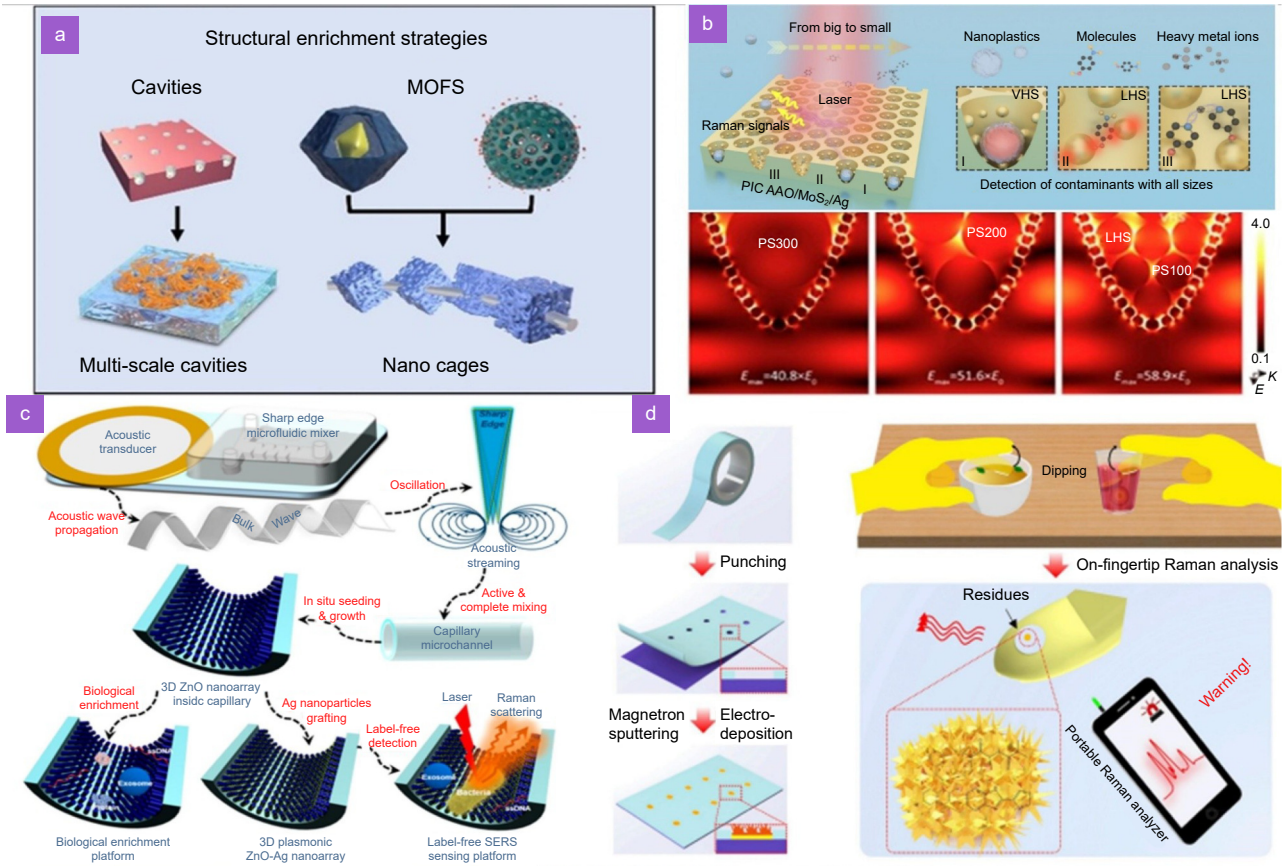

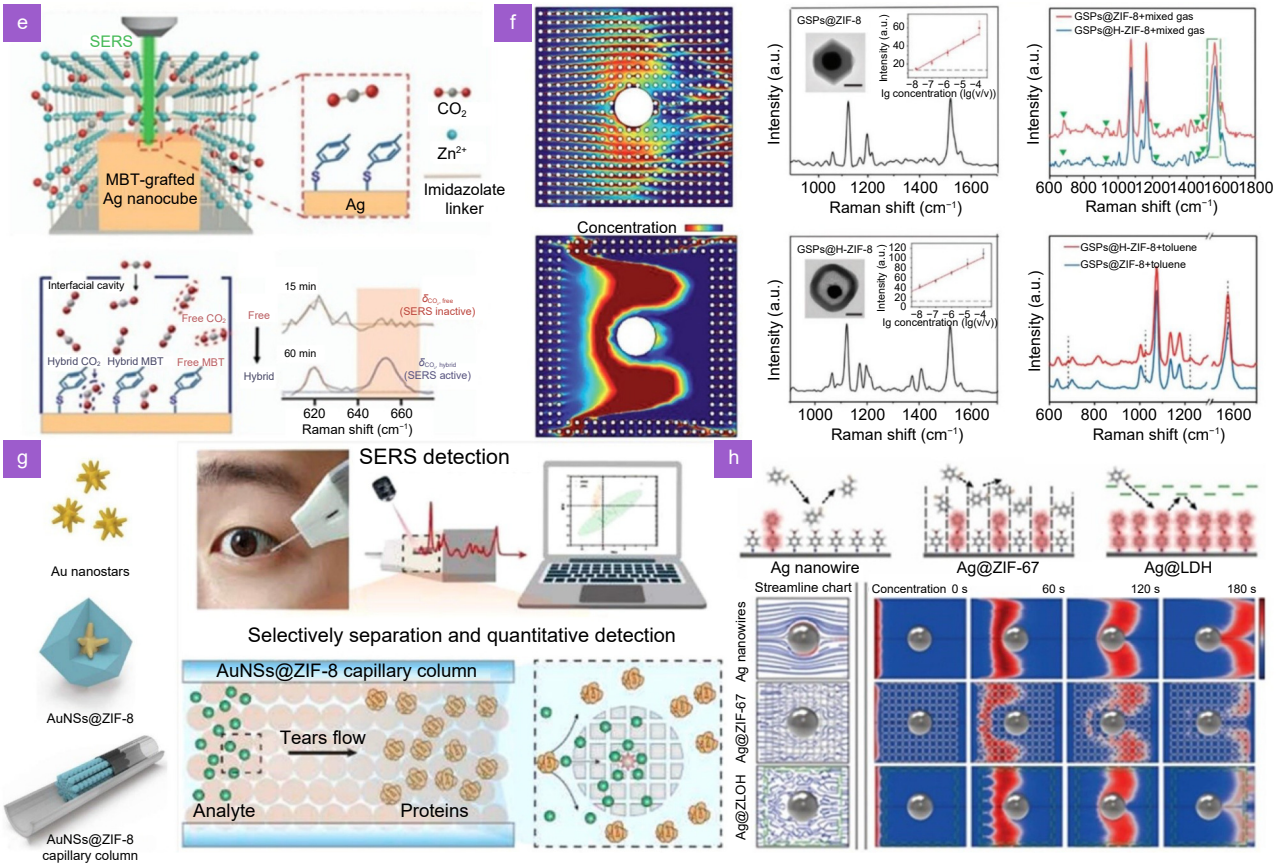

Fig. 6 | (**a**) Overview of structural enrichment strategies. (**b**) Passive cavity structure enrichment. A particle-MoS_2-coated cavity structure composed of AAO/MoS_2/Ag was designed for the enrichment and detection of mercury ions (Hg^{2+}), 4-aminobenzenethiol, and polystyrene nanoplastics, with simulations conducted on the electromagnetic field intensity. (**c**) Process design intent for the preparation of uniformly patterned and distributed arrays of zinc oxide nanostructures for active enrichment and detection of biomolecules using an acoustic fluidic device. (**d**) A capillary-based flexible multiscale cavity structure developed and attached to gloves for actively enriching solutions and identifying residual contaminants. (**e**) By integrating a ZIF-8 gas absorption layer on an array of Ag nanocubes, inert gas-liquid reactions were driven under ambient conditions, with SERS spectroscopy used to monitor the reaction process. (**f**) Hollow ZIF-8 coated on gold superparticles with a yolk-shell structure served as SERS substrates, while solid ZIF-8 SERS substrates acted as controls, for comparative simulation of gas flow rates and Raman performance tests. (**g**) A MOF-based SERS capillary column was developed for rapid, accurate, and reliable detection of MDA in tears. (**h**) Gas flow rate simulations were performed on hollow Co-Ni layered double hydroxide (LDH) nanocages and their control groups, demonstrating the superior gas-phase molecular capture ability of the former. Figure reproduced with permission from: (b) ref.[86], Copyright 2022 American Chemical Society; (c) ref.[91], Copyright 2020 American Chemical Society; (d) ref.[90], Copyright 2020 Elsevier; (e) ref.[89], Copyright 2017 American Chemical Society; (f) ref.[88], Copyright 2022 John Welly and Sons; (g) ref.[85], Copyright 2024 American Chemical Society; (h) ref.[83], Copyright 2019 John Welly and Sons.

analytes, restricting only when analytes fall within the cavity structures. Furthermore, the approach endows the platform with excellent versatility in liquid-phase detection but also presents drawbacks such as weaker enrichment effects and lower efficiency.

To overcome these limitations, it is essential to design substrates with active enrichment capabilities. The capillary effect, a fascinating mechanical phenomenon, is driven by the intricate interplay of surface tension, adhesion, and cohesion. This process allows liquids to spontaneously flow into narrow spaces, effectively capturing and concentrating analytes present within. From a substrate preparation perspective, those designed to exploit the capillary effect for active enrichment typically incorporate structures with different scales (collectively known as multi-scale or cascaded structures). Concretely, these structures are often created by combining microscale structures (such as bowls, pits, or capillaries) produced through physical imprinting or mold turning techniques with nanoscale structures synthesized by chemical methods[118]. To date, numerous studies have reported and validated the feasibility of this approach. For

instance, Huang et al. utilized an acoustofluidic device to fabricate a uniformly patterned array of zinc oxide nanostructures (Fig. 6(c)). Since this nanoarray coating is located within a glass capillary, it exerts active forces that can rapidly and effectively capture and enrich biomolecules ranging in size from a few nanometers to several hundred nanometers[91]. To enable the detection of these biomolecules, Ag nanoparticles were deposited on the ZnO nanoarray, yielding a ZnO-Ag capillary device that functions as a label-free plasmonic biosensing system. This system was applied for SERS detection of exosomes, DNA oligonucleotides, and Escherichia coli, facilitating sensitive and label-free analysis. In a separate example, Zhang et al. introduced an active enrichment strategy based on capillary-driven multi-scale cavity structures for detecting pollutants[90]. The preparation process of the substrate is illustrated in Fig. 6(d). Initially, gold nano dendrites-decorated microholes were created on a flexible conductive tape using a combination of physical punching, magnetron sputtering, and electrochemical deposition. This structure can be attached to wearable gloves, allowing for the rapid collection and immobilization of analytes from the original solution into SERS-active microholes through a simple "dip-pull" procedure, thereby enabling on-site identification of residual pollutants. Both aforementioned active physical enrichment strategies offer significant advantages in manipulating the behavior of liquid-phase molecules, demonstrating notably higher detection efficiency compared to passive physical enrichment strategies.

However, active enrichment strategies also suffer from two distinct drawbacks: 1) Limited detection sensitivity: In the context of low-concentration analytical solutions, the efficacy of these strategies is hindered in terms of the localization and concentration of the target molecule over a limited spatial domain. 2) Narrow scope of application: this strategy is dedicated to the realization of liquid-phase analyte enrichment, but suffers from serious shortcomings in the detection of gases. The primary rationale underlying this phenomenon pertains to the inherent dynamic nature of the gas phase, a characteristic that distinguishes it from both liquid and solid phases. In the gas phase, molecules possess augmented kinetic energy, a property that enables them to surmount intermolecular van der Waals forces. This heightened molecular mobility consequently renders the process of effectively adhering these molecules to the detection area more arduous.

To broaden the application to the gas phase and enable more precise analyte concentration, it is essential to develop SERS substrates featuring hollow structures and secondary adsorption properties. Metal-organic frameworks (MOFs), as porous crystalline structures formed by the connection of metal nodes and organic linkers, offer inherent advantages for the capture, sieving, and enrichment of gas molecules due to the enormous specific surface area (up to 7000 m^2/g) and regularly distributed lattice systems[36,88,92,119]. Conventional MOF-SERS substrates are created by depositing MOFs onto the surface of predetermined SERS-active metal nanoparticles[120]. For instance, Ling et al. facilitated inert gas-liquid reactions under ambient conditions by incorporating a zeolitic imidazolate framework-8 (ZIF-8, a branch of MOFs[121]) gas absorption layer onto an array of Ag nanocubes (as shown in Fig. 6(e))[89]. The introduced ZIF structure, with a pore size of 0.34 nm, selectively concentrates immiscible gaseous and liquid reactants, thereby facilitating molecular interactions at the solid-MOF interface. Moreover, the Ag component functions as a SERS-active layer, allowing for in situ monitoring of gas-liquid reactions at the molecular level. In a separate example, in order to accurately detect biomarkers in complex exhaled gases and to eliminate the interference of other components, Wang et al. proposed hollow ZIF-8 wrapped around gold superparticles with an egg yolk shell structure as a SERS substrate[88]. Similar to solid ZIF layers, the hollow ZIF-8 layer possesses the capability to concentrate gas molecules. These concentrated molecules subsequently interact with the functionalized surface of the superparticles, eliciting a robust response signal. However, unlike solid ZIF layers, the hollow ZIF layer can effectively exclude interfering molecules that are not bound to the modifier molecules. This leads to a detection limit that is 5-fold lower than that of core-shell structures (Fig. 6(f)).

As research advances, the application scenarios have expanded beyond the detection of gas-phase analytes. Recently, MOF-SERS substrates have been applied to the clinical diagnosis of disease biomarkers in tears (Fig. 6(g)). It is noticed that the limited volume of tear samples, the low concentration of biomarkers in tears, and the complex composition of tear fluid present significant challenges for precise testing. In response to these challenges, Feng et al. innovatively developed a novel MOF-based SERS capillary column that integrates in-situ separation and enrichment capabilities. This advancement enables the rapid, accurate, and reliable detection of

malondialdehyde (MDA) in tear samples. Concretely, the SERS substrate consists of a capillary designed for collecting tear fluid, filled with a mixture of nanoparticles comprising ZIF-8-coated gold nanostars (AuNSs). These components facilitate the enrichment, separation, and in-situ SERS detection of analytes. Meanwhile, the AuNSs are modified with 4-aminothiophenol, enabling Schiff base reactions with MDA. This design allows for the selective separation, enrichment, and in-situ detection of disease markers such as MDA in tear fluid, achieving a detection limit of 9.38×10^{-9} mol/L[85]. However, due to the affinity between the guest and the nanoporous material, several analytes are susceptible to be adsorbed on the cross-sites of the MOF scaffolds[117]. These adsorbed molecules will obstruct the fine channels, hindering the access of other target analytes to the hotspots surface. Consequently, such obstruction may lead to diminished detection sensitivity and compromised repeatability. To avoid this issue, it is necessary to develop other hollow framework structures with larger pore sizes and higher porosity. Hollow nanocage structures, which exhibit excellent gas interaction properties and are easy to prepare, have already been utilized in gas sensing applications. For instance, Wang et al. designed a hollow cobalt-nickel layered double hydroxide nanocage on Ag nanowires (Ag@LDH) to enhance the ability to adsorb gaseous molecules and reduce the probability of blockage[83]. As the simulation results in Fig. 6(h), when gaseous molecules moved through the LDH nanocages, the motion was interfered with and the molecules fell in whirlpool-like patterns of flow, moving back and forth around the centered Ag nanowires. As long as the LDH nanocages persist, the flow will continue to be irregular and result in increased drag, and particularly pressure drag, which is caused by the pressure differential between the front and rear surfaces of the object as gaseous molecules are trapped in the LDH nanocages. Therefore, the Ag@LDH demonstrated a significant improvement in gas adsorption compared to Ag and zeolitic imidazolate framework on Ag nanowires. This research direction holds promise for providing a simple and effective diagnostic strategy for the early detection of lung cancer.

In conclusion, integrating hollow or porous structures with SERS substrates indeed effectively enhances the selection and enrichment of target analytes, exhibiting unique advantages in the detection of both liquid-phase and gas-phase analytes. However, issues such as poor selectivity, easy depletion of analytes, and low reusability of the substrate remain significant challenges that constrain the further development of physical structure enrichment strategies.

It is worth noting that designing the substrate structure not only improves its ability to confine and screen analytes, but also changes its surface energy. This affects wettability, which is critical for the concentration and detection of aqueous analytes, and will be highlighted in the next section.

Wettability-related concentration strategies

Numerous studies have indicated that superhydrophobic surfaces (water contact angle greater than 150°) allow droplets to remain quasi-spherical during evaporation, thereby effectively reducing the solid-liquid contact area and allowing internal analytes to settle in a highly restricted area of a few square micrometers, with a concentration increase of up to 10^4 fold[93]. Therefore, in order to aggregate analytes and achieve efficient SERS detection, substrate design combining hydrophobicity properties with hotspot engineering is a feasible approach. However, conventional material surfaces are not naturally superhydrophobic (water contact angle less than 150°), which leads to solution dispersion on the surface, inevitably diluting the analytes inside.

Inspired by the morphology of natural organisms, researchers have discovered that surface morphology exerts a significant influence on wetting properties. For example, by mimicking the surface morphology of rose petals, substrates with micro-indentations and nano-protrusions were prepared. This strategy significantly enhanced hydrophobicity (water contact angle of 155°)[80] and provided an effective approach to localize the analyte in a tiny sensing region, which correspondingly increased the sensitivity of the SERS detection (down to a concentration of 10^{-14} M). In addition, inspired by the regularly arranged brush-like projections on the surface of lotus leaves, the array structure is also expected to yield excellent hydrophobic properties. As shown in Fig. 7(a), Zhou et al. prepared hierarchical plasmonic micro- and nano-arrays to concentrate dilute analytes in water droplets with the assistance of Leidenfrost evaporation (the controlled evaporation process that occurs when a liquid droplet interacts with a surface significantly hotter than the liquid's boiling point, inducing the Leidenfrost effect. This phenomenon is characterized by the formation of an insulating vapor layer beneath the droplet, which alters the dynamics of heat transfer and

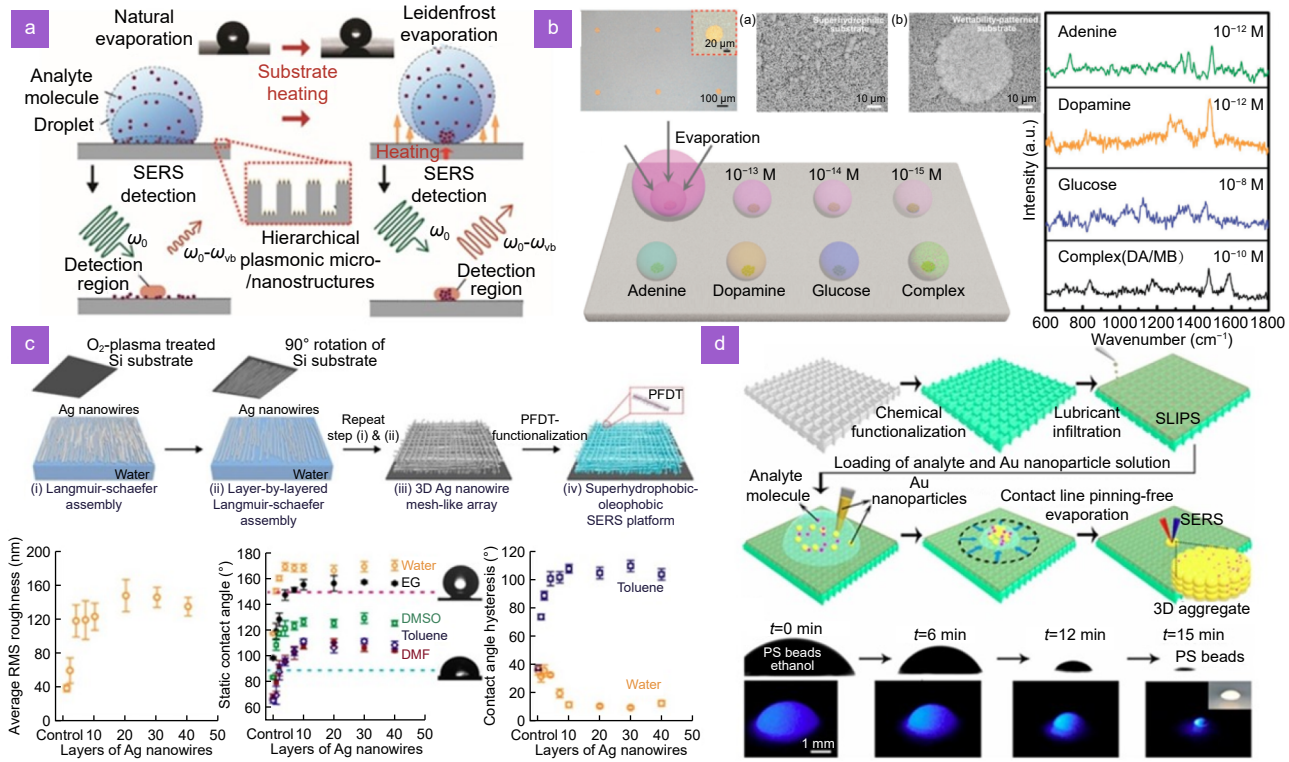

Fig. 7 | (**a**) Schematic illustration of the principle for preparing hierarchical plasmonic micro/nanoarrays for SERS detection, utilizing Leidenfrost evaporation to concentrate diluted analytes within water droplets. (**b**) Schematic representation of the morphology and working area of patterned superhydrophobic-superhydrophilic substrates, along with high-throughput SERS spectra for multiple analytes. (**c**) Schematic depiction of the fabrication process for a superhydrophobic-oleophobic (SHP-OP) three-dimensional silver nanowire mesh SERS platform, including characterization of the hydrophobic and oleophobic properties of the target substrate and control groups. (**d**) Schematic illustrating the principle of SLIPSERS for enriching any analyte from common liquids, along with optical images showing the actual evaporation process of droplets on the SLIPSERS substrate. Figure reproduced with permission from: (a) ref.[82], Copyright 2020 American Chemical Society; (b) ref.[87], Copyright 2018 John Welly and Sons; (c) ref.[84], Copyright 2014 American Chemical Society; (d) ref.[122], Copyright 2016 National Academy of Sciences.

evaporation compared to conventional boiling.) and achieved ultra-sensitive SERS detection[82]. The natural hydrophobicity angle of the substrate reaches 140° without any modification, which greatly reduces the area for final deposition. Subsequently, the hydrophobic angle was further increased to 170° at a heating environment of 120 °C due to the unique nature of the array structure, which successfully realized the switching between the Wenzel and Cassie states. Specifically, by precisely controlling the evaporation process, the central region of the droplet was immobilized on the micro- and nano-structures, while the surrounding regions were suspended by vapor convection. In this case, the analytical droplet can continuously shrink towards the immobilized center point, thus minimizing the analyte deposition area and enabling ultra-fast and ultra-sensitive SERS detection without any additional surface treatment.

In addition to utilizing a single hydrophobic property for analyte concentration and SERS detection, patterned SERS substrates with both hydrophobic and hydrophilic properties have been increasingly investigated in recent years. The combination of hydrophobic and hydrophilic properties not only allows for more effective control of liquid flow and positioning, but also enhances the sensitivity and reliability of detection by optimizing the distribution of the pattern. By precisely regulating the hydrophobic and hydrophilic regions of the substrate, it is possible to achieve efficient capture and concentration of analytes, thus improving the quality of SERS signals and providing a more flexible and powerful solution for diverse, high-throughput detection requirements. For instance, a SERS microchip of Au-areoles array, mimicking the areole on the cactus, is facilely and controllably prepared through selectively electrochemical deposition on patterned superhydrophobic–superhydrophobic substrates (Fig. 7(b))[87]. The Au-areoles are full of SERS hotspots owing to the large amounts of sharp edges, tips, and coupled branches. Meanwhile, the superhydrophobic

sites on the superhydrophobic substrate can collect the target molecules into those hotspots. The combination of the SERS enhancement of the nano structured-Au and the collective effect of the superhydrophobic-superhydrophilic pattern endows the microchip with sample-effective, ultrasensitive, and efficient Raman detection capabilities, which are demonstrated by integrated detection of femtomole Rhodamine 6G and diverse bioanalyses. The chip can also be used for mutually independent multisample detection without interference.

The aforementioned hydrophobic concentration strategies are only capable of enriching analytes in aqueous solutions and lack restrictions on substances dispersed in organic solvents with low surface tension, e.g., a substrate with superhydrophilicity alone is not capable of effectively concentrating analytes dispersed in oil-phase solvents, which are commonly found in the production of living and natural environments. Therefore, it is necessary to simultaneously investigate the oleophobic properties of substrates to broaden the application scenarios. In recent years, a large amount of work has been presented on the preparation of superhydrophobic-oleophobic substrates and the integrated detection of multiphase analytes. For instance, Ling et al. prepared a superhydrophobic-oleophobic (SHP-OP) three-dimensional silver nanowire mesh SERS substrate, which successfully solved the random diffusion problem and realized ultra-trace toxin detection in aqueous and organic liquids[84]. As shown in Fig. 7(c), the substrate was first assembled layer-by-layer with silver nanowires to form a highly roughened and non-close-packed 3D mesh structure, and then functionalized with perfluoro decanethiol to obtain the non-wetting properties. The results indicated that the contact angles reached 170° and 112° for water and toluene (surface tension of 72.7 and 28.5 $mN{\cdot}m^{-1}$, respectively). These non-wetting phenomena resulted in a 100 fold and 10 fold enrichment of water- and toluene-soluble analytes. Subsequently, with only 1 μL of analyte solution, melamine and Sudan I were quantitatively and ultra-trace detected down to 0.1 fmol in water and toluene (10^3 fold lower than the specified detection limit), clearly demonstrating the SHP-OP SERS platform is an attractive and ultrasensitive toxin sensor. Although this work enabled the preparation of oleophobic SERS substrates, it is still challenging to experimentally prepare SERS platforms that exhibit both superhydrophilicity and superoleophobicity.

In addition to superhydrophobic-oleophobic SERS platforms, smooth liquid-injected porous surfaces (SLIPS) are emerging strategies for SERS detection in non-aqueous solvents and biological fluids. Unlike superhydrophobic/oleophobic surfaces with solid-vapor-liquid three-phase contact, a smooth and homogeneous liquid-liquid interface can be formed by injecting a liquid into a layered structure. SLIPS was first proposed by Wong et al. in 2011[81]. Subsequently, a large number of papers on SLIPS have emerged. Although the water contact angle, which is related to the hydrophobicity of the surface, is much less than 150° on SLIPS, it indeed possesses excellent liquid repulsion, which is related to the contact angle hysteresis or sliding angle. As a result, this approach offers significant advancements in various fields such as drag reduction, anti-icing, anti-fouling, and anti-corrosion. In conjunction with SERS (SLIPSERS), it manifests distinctive benefits in the enrichment and sensing of liquid-phase analytes.

As shown in Fig. 7(d), in SLIPSERS[122], a perfluoro liquid is first infiltrated into the nano-extruded Teflon membrane. This perfluoro liquid acts as a lubricant and possesses the property of being insoluble in a wide range of aqueous and organic solvents. Next, droplets containing analytes and plasma nanoparticles are introduced on the surface of this membrane, where solvent pinning will not occur due to the special properties of the Teflon membrane. As a result, these droplets will gradually evaporate in a stable contact angle pattern until completely dry. This process results in the formation of a three-dimensional structure containing approximately 2,000 gold nanoparticles intertwined with analyte molecules and containing this combination of structures in every square millimeter. At the same time, the SLIPSERS platform demonstrates excellent detection capabilities, the limit of detection for R6G (Rhodamine 6G) in ethanol solution can reach as low as 1 amolar, which corresponds to approximately 30 R6G molecules per 50 mL of solution. In addition, the platform is capable of quantifying a wide range of soluble analytes in the submolar concentration range, including biological species (bovine serum albumin) and environmental contaminants (bis (2-ethyl-hexyl) phthalate).

While innovative, the key concerns in this strategy lie in the need to select suitable lubricating liquids that fulfil several criteria, including good adherence within the porous support, immiscibility with sample droplets, sufficient non-volatility for efficient concentration of analytes/particles and most importantly, without the

generation of interfering SERS signals. Moreover, this platform only works for liquid-soluble analytes and is unsuitable for the direct enrichment of gaseous and/or volatile chemical species for SERS sensing.

In summary, the establishment of non-wetting SERS strategies aims to provide specialized treatment methods for the enrichment and concentration of liquid-phase analytes. However, this approach lacks the capability to detect gas-phase and solid-phase analytes, making its advantages and limitations equally evident.

Macroscopic force field enrichment strategies

Thus far, our discussion of various SERS enrichment strategies has primarily focused on chemical strategies involving the functional groups modification or physical strategies centered on structural design. Both approaches emphasize substrate preparation and rely heavily on the interactions between the substrate and analytes. However, it is important to note that these processes invariably result in analyte depletion, making it challenging to concentrate all target molecules from both the liquid and gas phases. Furthermore, the presence of false-negative results becomes a concern when the analyte concentration is exceedingly low. Consequently, to enhance detection accuracy and reduce costs, reliance on substrate design and preparation alone is inadequate.

Macroscopic force field assisted enrichment

In recent years, a number of studies have centered on the subject of assisting and regulating the enrichment state of analytes on the surface of SERS substrates through macroscopic forces or fields (magnetic/acoustic). The assistance and induction of the macroscopic force field has been demonstrated to allow for a more stable contact process between the analyte and the SERS substrate. This approach will be explored in detail with three concrete examples of work that follows.

1) External magnetic field-assisted active enrichment strategy[96]: conventional enrichment methods usually rely on passive molecular adsorption, which leads to low capture probability and long capture duration. To address this issue, controlling the movement of hotspots and thus actively capturing analytes is a feasible approach. Therefore, the concept of "moving hotspot" has been proposed to realize ultrasensitive SERS sensing by combining the strengths of hotspot engineering and active molecular enrichment. For example, the outer wall of a micromotor is modified with a high density of equipartitioned excitonic nanostructures as a way to stimulate the generation of hotspots through nanoimprinting and rolling origami techniques (Fig. 8(a1)). Such micromotors with nanostructured outer walls are called hierarchical structured micromotors (HSMs). At the same time, a layer of iron elements is added to the wall of the HSM to realize controlled motion in an external magnetic field. Its surface dense hotspots can actively enrich molecules in the fluid by magnetic force (Fig. 8(a2)). It was found that the active enrichment approach of HSM could effectively accelerate the molecular adsorption process, and the increase in the number of molecules near the hotspot led to a significant enhancement of the SERS intensity (Fig. 8(a3)). This "motional hotspot" strategy provides a viable approach for designing high-performance SERS substrates. In addition, this idea enables the customization of the tube length, tube diameter, and the surface pattern of the outer wall of HSMs, which facilitates the construction and customization of micromotors for different application scenarios.

2) External magnetic field-assisted chemical enrichment strategy[102]: typically, magnetic materials polymerize in the presence of an external magnetic field. Utilizing this property, combining noble metal nanoparticles with paramagnetic nanomaterials and chemically modifying their surfaces can enhance the enrichment ability of the substrate and facilitate detection. For example, a novel SERS-based magnetic immunosensor was designed to detect intact but inactivated H_3N_2 influenza viruses by constructing a sandwich composite structure consisting of a SERS marker, a target influenza virus, and a highly SERS-active magnetic support substrate (Fig. 8(b1)). The magnetic support substrate greatly simplifies the process of sample pretreatment as it allows for the enrichment and isolation of viruses from complex matrices. Utilizing a portable Raman spectrometer and assisted by an external magnetic field, the detection performance of this immunosensor was significantly enhanced (Fig. 8(b2)), which could detect H_3N_2 viruses as low as 10^2 TCID50/mL (TCID50 refers to the infectious dose in tissue culture at the 50% endpoint), with a good linearity between 10^2 and 5×10^3 TCID50/mL. Considering its time efficiency, portability, and sensitivity, this SERS-based magnetic immunoassay is highly promising as a point-of-care assay in clinical and diagnostic practice.

3) Ultrasound-assisted self-assembly enrichment strategy[98]: Due to the difficulty for target molecules to enter the hotspot regions of traditional noble metal nanoparti-

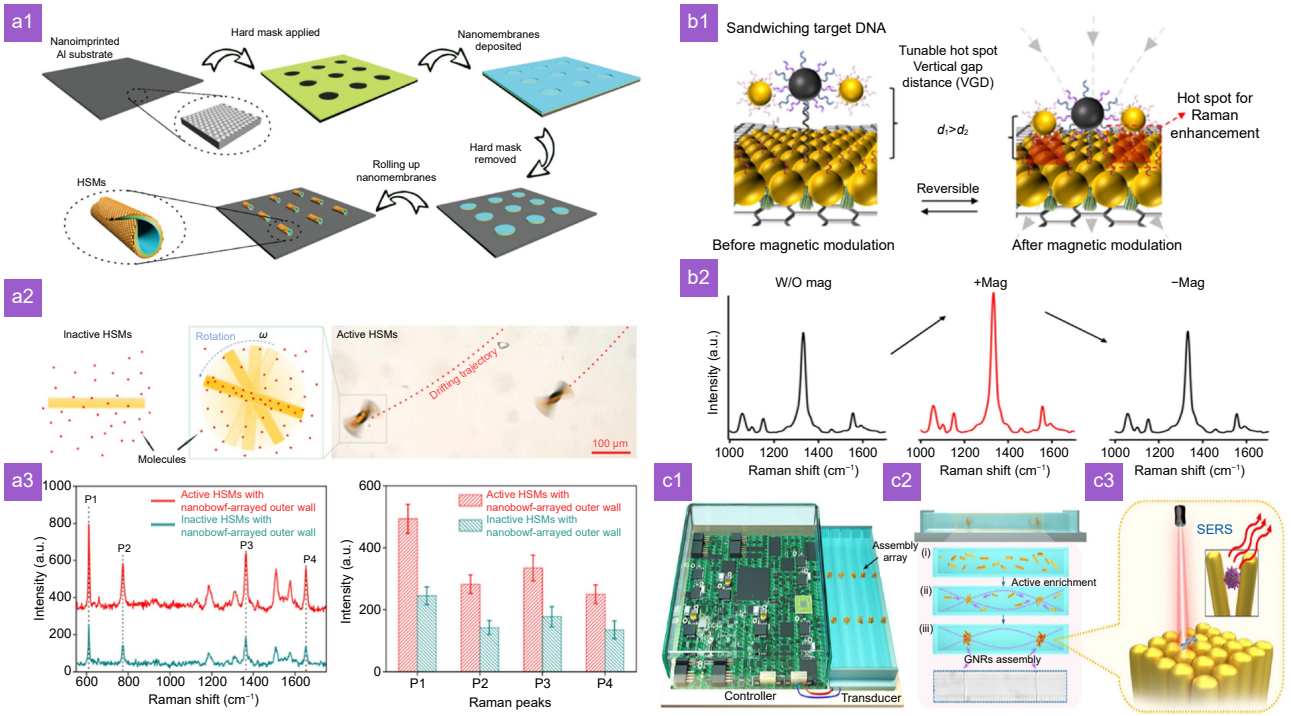

Fig. 8 | (**a1**) Schematic illustration of the procedure for fabricating HSMs (Hierarchical structures with magnetics) using rolling origami. (**a2**) Left: schematic diagrams illustrating the principles of passive and active enrichment by HSMs. Right: optical images of magnetic force-driven HSM during active molecular enrichment. (**a3**) SERS spectra obtained from inactive and active HSMs after molecular enrichment (concentration of R6G is 5×10^{-8} M), along with a histogram of SERS intensity for characteristic Raman peaks of R6G. (**b1**) The Raman signal can be enhanced by reducing the vertical gap distance between DTNB/DNA4-AuNPs and AuNPs on the AuNP-rGO-SW through downward magnetic attraction. Removing the magnetic modulation can reverse the formation of hotspots and restore the original Raman signal, thereby constructing a reversible platform. (**b2**) SERS spectra under +Mag or −Mag conditions when detecting 1 nM N-cDNA. (**c1**) Schematic illustration of a fully integrated active enrichment platform. (**c2**) Active enrichment of gold nanorods in a nanoliter (10^{-7} L) sample. (**c3**) Schematic showing the aggregation of gold nanorods at assembly positions for SERS detection. Figure reproduced with permission from: (a) ref.[96], Copyright 2020 American Chemical Society; (b) ref.[102], Copyright 2022 American Chemical Society; (c) ref.[98], Copyright 2023 American Chemical Society.

cles, ultrasound is chosen to manipulate nanoparticles, thereby actively enriching and encapsulating analytes without damaging them. This active enrichment can detect ultra-low concentrations of nucleic acids without the need for the relatively time-consuming polymerase chain reaction (PCR), representing a significant direction for the future of rapid nucleic acid detection. This method has been applied to the detection of COVID-19. Zhang et al. reported an integrated active enrichment platform capable of directly detecting COVID-19 nucleic acids in nanoliter samples without PCR using a handheld device. The platform consists of a capillary-assisted liquid sampling system, an ultrasonic output integrated circuit system, and a mobile phone-based SERS system (Fig. 8(c1)). Considering acoustic responsiveness and SERS enhancement performance, gold nanorods were selected for biomedical applications. Functionalized gold nanorods effectively capture and enrich biomarkers under ultrasound-induced aggregation (Fig. 8(c2)). This method can actively aggregate gold nanorods within 1–2 seconds and achieve highly sensitive SERS detection of COVID-19 biomarkers in nanoliter (10^{-9} L) samples within 5 minutes, with a sensitivity of 6.15×10^{-13} M (Fig. 8(c3)). Additionally, it holds potential for detecting throat swab samples.

The three aforementioned studies utilize macroscopic force fields to assist and regulate the binding process between SERS substrates and analytes, resulting in platforms that integrate enrichment and detection. Compared to conventional physical and chemical enrichment strategies, these approaches offer higher detection efficiency, accuracy, and applicability.

Macroscopic force field direct enrichment — magnetic/acoustic levitation system

With further research on macroscopic force fields, a large number of works have revealed and confirmed that

macroscopic force fields (acoustic or magnetic) possess the ability to directly manipulate analytes, allowing analytes with the same physical properties (density, mass, size, etc.) to reach a stable state of mechanical equilibrium (levitation) and to aggregate at the equilibrium position. These strategies of enrichment do not introduce an interference term, requires the construction of a stable force-field environment, and enables lossless enrichment of analytes under certain circumstances.

Acoustic levitation, as one of the most typical mechanical lossless enrichment methods, has been successfully combined with Raman spectroscopy. Acoustic levitation utilizes the force of acoustic radiation to levitate objects in a variety of media (e.g., air, soil, solution). Solidification of metals, non-contact transport of substances, droplet dynamics and analytical chemistry have been studied for decades, and in 2003, Prof. Lendl's group and Prof. Nilsson's group used SERS to monitor chemical reactions and crystallization processes within suspended droplets, respectively[124–125]. In 2022, Yang et al. reported the lossless enrichment of analyte molecules dissolved in any volatile liquid, attached to solid objects, or dispersed in air using an acoustic levitation platform (Fig. 9(a1–a4))[95]. The results indicate that Au nanoparticles can be concentrated concurrently with analytes in different phases to achieve sensitive SERS detection, even at attomole (10^{-18} mol/L) concentration levels. This is a breakthrough that bypasses the complex platform preparation process and avoids analyte depletion while enabling reproducible detection with higher sensitivity. In addition, the construction of the acoustic levitation platform breaks the selectivity and limitation of traditional enrichment platforms for analyzed species, and the highly generalized detection equipment is obviously more valuable and promising for application. More importantly, the acoustic levitation platform is compatible with most microsensing technologies. For instance, acoustofluidics, which is the integration of acoustics and microfluidics, has recently received increasing research attention across multiple disciplines, partly due to its capabilities for non-contact, biocompatible, and precise manipulation of micro- and nano-objects[123, 126]. Leveraging this capability, Tony Jun Huang and colleagues developed an acoustofluidic-assisted dual-mode sensing platform capable of performing both immuno-fluorescence and SERS-based dual-mode detection (Fig. 9(b1))[127]. In this platform, acoustofluidics is used to concentrate silica nanoparticles coated with relevant target molecules at different positions within a square glass capillary, achieving signal amplification (Fig. 9(b2)). By concentrating fluorescent analytes and functionalized nanoparticles towards the center of the glass capillary, the output fluorescence signal is significantly enhanced, thereby boosting the performance of the immunoassay. Simply by adjusting the input frequency, analytes conjugated with silica nanoparticles can also be focused on the edges of the capillary microchannel, allowing them to interact with the surface's plasmonic zinc oxide-silver nanorod arrays. This dual functionality can be applied to a variety of biological samples using mechanisms similar to those based on immuno-fluorescence or SERS detection. Based on these two sensing modes, the platform successfully detects the presence of biomarkers even at extremely low concentrations (as low as tens of exosomes per μL), as shown in Fig. 9(b3).

Through acoustic levitation, lossless enrichment of analytes in different phases can be realized, and effective detection is possible even at extremely low concentrations. In addition, the construction of the acoustic levitation platform breaks the limitations of traditional enrichment platforms and boasts a high degree of versatility and applicability. The incorporation of acoustic fluidic technology further expands the application scope of this platform, enabling dual-mode detection based on immunofluorescence and SERS through precise manipulation of micro/nano objects. This technology exhibits great potential in various fields, including biomedicine, environmental monitoring and chemical analysis, and hold great promise for future scientific research and practical applications.

Similar to acoustic levitation, magnetic levitation (Maglev) technology, which relies on competing gravitational and magnetic forces and a paramagnetic solution possessing a continuously varying density gradient in a magnetic field, is also expected to enable the lossless enrichment of analytes[97]. In particular, Maglev allows for the separation of magnetic particles suspended in a medium based on their density, which is difficult to achieve with acoustic levitation. Currently, magnetic levitation technology has been demonstrated and applied in food analysis, detection of banned substances, protein-ligand interactions, monitoring of chemical reactions, and as a detection step in immunoassays.

The most common magnetic levitation system, referred to as the "standard" system, employs two solid permanent magnets with like poles facing each other (either

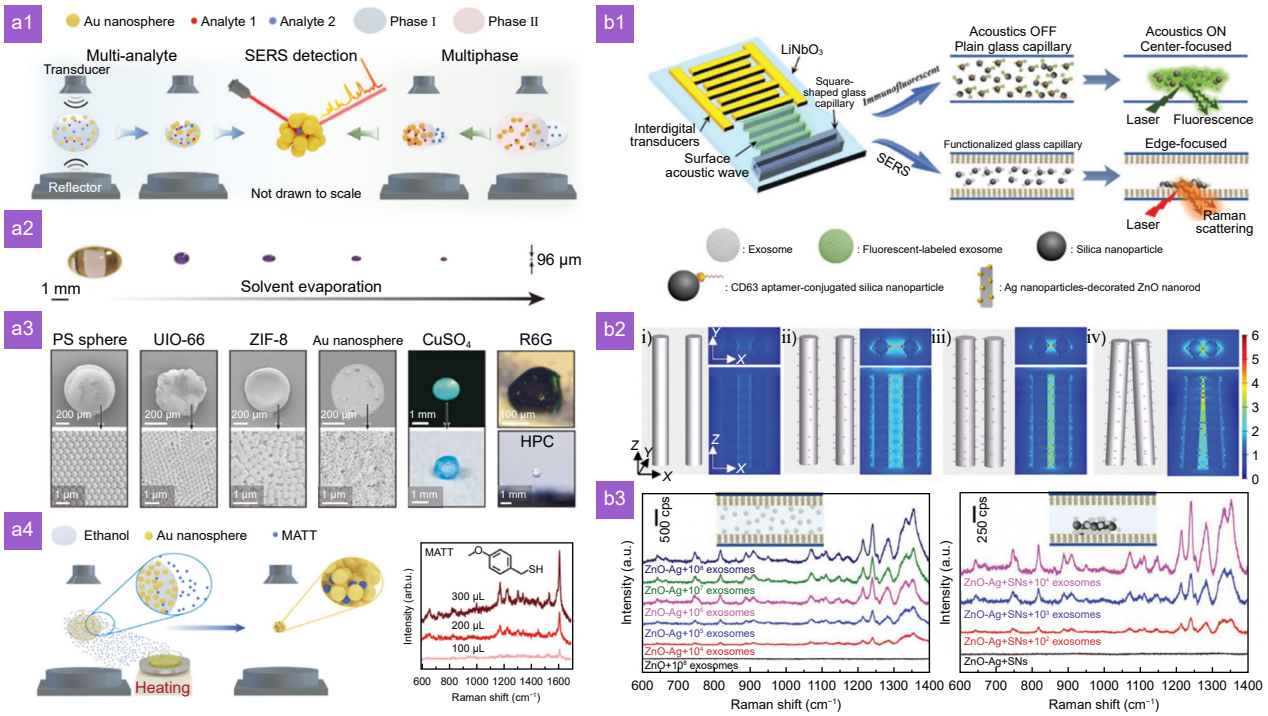

Fig. 9 | (**a1**) Schematic illustration of multiplex and multi-phase enrichment of multiple analytes using the DLE (Droplet-based liquid enrichment) platform followed by subsequent multiplex and multi-phase SERS detection. (**a2**) Process of enriching CV molecules from a 10 μL ethanol solution using acoustic levitation. (**a3**) Aggregates concentrated from a 10 μL dispersion containing 500 nm polystyrene spheres, 300 nm ZIF-8 octahedra, UIO-66 dodecahedra, 50 nm gold nanospheres, $CuSO_4$ and R6G aqueous solutions, and HPC ethanol solution. (**a4**) Left: Schematic for capturing, enriching, and performing SERS detection of airborne molecules using the DLE platform; Right: SERS spectra of MATT molecules captured and enriched from air by an ethanol droplet composed of gold nanospheres. The MATT molecules in the air were generated by heating MATT liquid 10 cm away from the suspended ethanol droplet. (**b1**) Schematic illustration of the working mechanism of an acoustofluidic biosensor. The dual-mode platform functions to concentrate target analytes at the center or periphery of a glass capillary using surface acoustic waves. (**b2**) FDTD simulations showing electromagnetic field distributions for different nanoarray structures: i) Original nanorods with a spacing of 200 nm, exhibiting limited electromagnetic field enhancement; ii) ZnO-Ag nanorods with a spacing of 200 nm, showing stronger electromagnetic field enhancement; iii) ZnO-Ag nanorods with a spacing of 100 nm, further amplifying electromagnetic field enhancement; iv) Tilted proton nanorods aggregated at both ends, demonstrating significant electromagnetic field enhancement. (**b3**) Left: SERS spectra of exosomes using a ZnO-Ag capillary without silica particle assistance, ranging from 10^4 to 10^8 μL^{-1} in concentration; Right: SERS spectra of exosomes detected using nanoparticle-assisted acoustofluidics method at concentrations of 10^2 to 10^4 μL^{-1}. Figure reproduced with permission from: (a) ref.[95]. Copyright 2022 Springer Nature; (b) ref.[123], Copyright 2020 John Welly and Sons.

N/N or S/S, with no difference in outcome) (Fig. 10(a1, a2)). This setup is similar to a spike trap or anti-Helmholtz configuration, which uses a pair of coaxially aligned identical electromagnetic coils with like poles facing each other, and the coil spacing equal to the coil radius. In experiments, two identical neodymium-iron-boron (NdFeB) permanent magnets (typically dimensions: 50 mm × 50 mm × 25 mm) are placed coaxially (with faces aligned and parallel), with like poles facing each other, at a distance of d=45 millimeters apart. Then, the center axis of the magnet is usually aligned so that it is parallel to the gravity vector. In this configuration, the forces acting on a particle suspended within the system can be described by the following equation[128]:

$$\boldsymbol{F}_{\rm g}+\boldsymbol{F}_{\rm m}=(\rho_{\rm s}-\rho_{\rm m})V\boldsymbol{g}+(\chi_{\rm s}-\chi_{\rm m})\mu_0 V(\boldsymbol{B}\cdot\nabla)\boldsymbol{B}=0, \quad (2)$$

$$\rho_{\rm s}=\alpha h+\beta\,, \quad (3)$$

here, $\boldsymbol{F}_{\rm m}$ is the magnetic force exerted on the levitated object due to its interaction with the magnetic field and the surrounding paramagnetic medium. $\rho_{\rm s}$ is the density of the object; $\rho_{\rm m}$ is the density of the paramagnetic medium; V is the volume of the object; $\boldsymbol{g}$ is the gravitational acceleration (with $||\boldsymbol{g}||$ being 9.80665 ms^{-2} on Earth); $\chi_{\rm s}$ is the magnetic susceptibility of the object; $\chi_{\rm m}$ is the magnetic susceptibility of the paramagnetic medium; μ_0 is the permeability of free space; $\boldsymbol{B}$ is the magnetic field; ∇ is the del operator; α (noted twice in the original text, likely a typographical error) represents coefficients

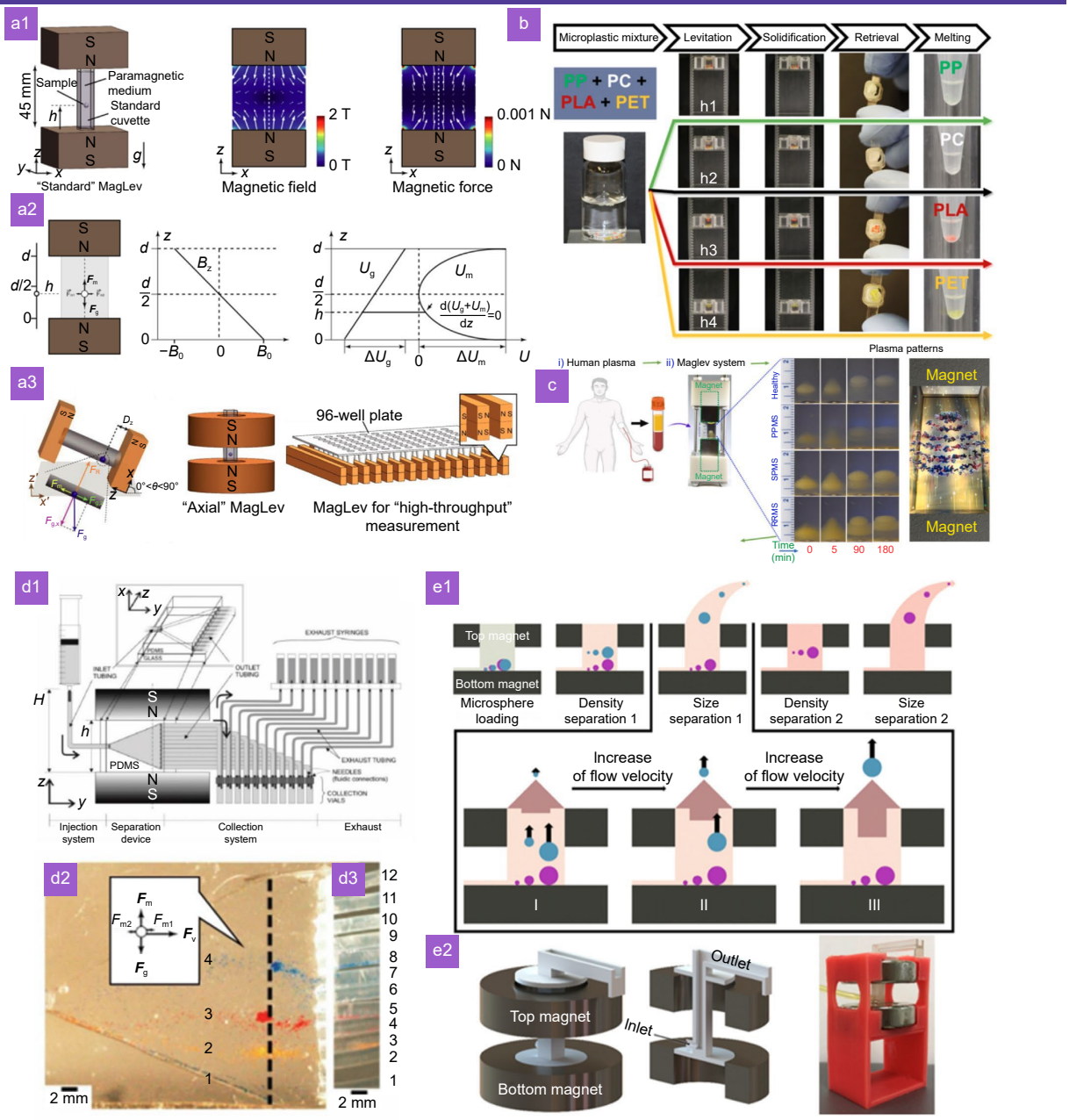

Fig. 10 | (**a1**) From left to right: schematic of a standard magnetic levitation system. Magnetic field distribution between two magnets, with a vertical dashed line indicating the central axis for object levitation. Simulation of the magnetic force experienced by a 5 mm glass bead suspended in a standard magnetic levitation system. (**a2**) From left to right: force analysis diagram of target particles suspended in a magnetic field. approximate linear magnetic field along the central axis of a standard magnetic levitation system used to suspend objects in paramagnetic media. gravitational potential energy and magnetic energy of levitated diamagnetic objects in a standard Maglev system, ΔU_g represents the change in gravitational potential energy (with zero energy defined at an infinite distance), and ΔU_m represents the change in magnetic potential energy (with zero energy defined at the midpoint between the magnets). (**a3**) From left to right: tilted magnetic levitation device. Axial magnetic levitation device. high-throughput magnetic levitation screening device. (**b**) In a standard magnetic levitation system, different density microplastic particles are sequentially floated by moving the tube position, and various types of microplastics are separated and captured using biphasic media. (**c**) Time-lapse photographs showing the separation of human plasma using a standard magnetic levitation system. (**d1**) Fluid flow perpendicular to the magnetic field gradient. A bead suspension (containing 250 mM GdCl3) flows into a V-shaped channel fabricated within a PDMS-based microfluidic device. (**d2**, **d3**) Beads are divided into four sections based on density and exit through outlet channels. (**e1**) Schematic illustration and working principle of a prepared two-dimensional magnetic levitation separation device. (**e2**) Photographs of the components of this two-dimensional magnetic levitation separation device. Figure reproduced with permission from: (a) ref.[97], Copyright 2020 John Welly and Sons; (b) ref.[99], Copyright 2022 American Chemical Society; (c) ref.[129], Copyright 2023 Elsevier; (d) ref.[100], Copyright 2007 American Chemical Society.

describing linear functions; h is the levitation height of the object. As understanding of this equation deepens, a wider variety of magnetic levitation devices have been developed and put into use (Fig. 10(a3)), which will not be described in detail here.

Recently, magnetic levitation has been applied to the separation of mixed waste plastics. By combining the linear density gradient provided by magnetic levitation with the step gradient offered by aqueous multiphase systems, additional functionalities for plastic enrichment and separation can be achieved. In experiments, simply adjusting the height of the container between the two magnets allows the aqueous multiphase system to selectively capture different plastics at the formed interfaces (Fig. 10(b))[99]. In another example, magnetic levitation technology has also been utilized for the separation and detection of human plasma components, facilitating early disease screening. As shown in Fig. 10(c), within a standard magnetic levitation system, human plasma is separated into multiple ellipsoidal bands in a solution of appropriately concentrated superparamagnetic iron oxide nanoparticles (SPIONs)[129]. To investigate whether the biomolecular composition of suspension elliptic bands is related to the health status of plasma donors, researchers used plasma from people with various types of multiple sclerosis (MS) as a model disease of clinical importance. The study results indicated that while there was little variation in protein composition, there were significant differences in the lipidomic and metabolomic profiles of each magnetically levitated ellipsoidal band. By comparing the lipidomic and metabolomic compositions across various plasma samples, it became evident that the levitated biomolecular ellipsoidal bands indeed contain information about the health status of the plasma donors. More specifically, each layer within a specific plasma pattern contained particular lipids and metabolites that played a significant role in distinguishing different subtypes of multiple sclerosis, namely relapsing-remitting MS, secondary progressive MS, and primary progressive MS. These findings pave the way for utilizing Maglev-based recognition of biomolecules in the discovery of biomarkers to identify and differentiate diseases.

Since the enrichment process occurs in solution, magnetic levitation enrichment methods are also compatible with most fluidic technologies. It has been reported that magnetic levitation systems can form stable density gradients in flowing fluids, thereby possessing unique separation characteristics that cannot be achieved using acoustic levitation methods. Here, we will discuss two spatial arrangement modes of fluid flow relative to the magnetic field gradient: 1) fluid flow perpendicular to the magnetic field gradient, and 2) fluid flow parallel to the magnetic field gradient. When the fluid flow is perpendicular to the magnetic field gradient, the viscous drag force on objects in the fluid (generated by fluid shear stress) is orthogonal to the physical forces (magnetic force, buoyancy, and gravity). Therefore, the lateral flow has minimal impact on the longitudinal gradient distribution of particles. This flow pattern, which resembles laminar flow, tends to cause lateral displacement of particles with negligible effect on their levitation height. As shown in Fig. 10(d1), the fluid flow direction is perpendicular to the magnetic field gradient, and four magnetic response beads of different densities are injected into a V-shaped tube fabricated from PDMS and reach equilibrium states within a standard magnetic levitation system. Since the perpendicular flow does not affect the particles' levitation height, the beads are pushed toward different outlets by viscous drag forces (Fig. 10(d2, d3))[101].

When the fluid flow is parallel to the magnetic field gradient, suspended objects experience viscous drag forces in the same direction as the magnetic field. This additional force disrupts the equilibrium that objects have in a static environment and moves them to a new position. At this new position, the strength of the magnetic force increases to counterbalance the viscous drag. In laminar flow, the magnitude of the viscous drag force on a standard sphere follows the formula[100]:

Notably, the magnitude of the viscous drag force on a particle is proportional to its radius. Therefore, for a flow system parallel to the magnetic field, the levitation characteristics of objects are influenced by both their density and size. In other words, as long as an appropriate flow rate is maintained, the system can simultaneously separate substances of different densities and sizes. For instance, integrating a standard magnetic levitation system constructed with two ring magnets with a separation chamber nested within and connected to a programmable pump (Fig. 10(e2)) enables two-dimensional separation of microplastics. The first dimension of separation is based on the continuous increase in the concentration of paramagnetic salt ($MnCl_2$), which achieves magnetic levitation of microplastics with specific densities. The second dimension is based on increasing the flow rate gradient while maintaining a constant $MnCl_2$

concentration, thereby classifying the magnetically levitated microplastics according to their different particle sizes (Fig. 10(e1)). Thus, microplastics are collected through their progressively increasing density, and particles corresponding to each density are then classified from smaller to larger sizes.

In summary, magnetic levitation integrates enrichment and separation with inherent advantages in specific selection. The integration of magnetic levitation enrichment with Raman detection may be a novel and feasible strategy. On the one hand, this simultaneous separation and enrichment process serves to avoid the interference of complex environmental impurities with the analytes; on the other hand, this nearly lossless enrichment process provides the foundation for Raman quantitative detection. However, to date, this technique has not been combined with Raman detection, primarily due to its own limitations: 1) Size limitations: theoretical analysis and experimental studies have determined that the standard Maglev system can stably levitate particles down to a minimum size (with a radius of approximately 2 μm). Particles with a radius smaller than ~2 μm tend to remain as a dispersed cloud in a standard magnetic levitation system due to Brownian motion. For example, Demirci used millimeter-sized Maglev systems to capture or levitate cells (such as bacterial and yeast cells). However, stably suspending individual bacterial cells in an aqueous paramagnetic medium requires a significant amount of time (several hours). Thus, under ambient conditions, it is challenging to rapidly levitate small particles (less than 1 μm) using simple magnetic levitation systems unless the spacing between magnets is reduced or the magnetic field strength is increased, both of which enhance the magnitude of the magnetic field gradient. 2) High detection difficulty: since the enrichment of analytes occurs within the solution, conventional SERS detection methods cannot be directly applied. This necessitates optimization of the magnetic levitation setup or the use of fiber-optic SERS probes for detection.

In addition to the two aforementioned syrategies, in recent years, optical tweezers technology has emerged as a significant contender in the domain of SERS enrichment[130–132], owing to its capacity to manipulate analytes and hotspots in a simultaneous manner. Notably, a single-beam enrichment system has been increasingly employed in SERS detection. This system employs a single-beam optical trap to concentrate free silver nanoparticles within a photofluidic chip, thereby substantially enhancing SERS performance. Experimental results demonstrate that the intensity of the Raman signal in the optically trapped state is markedly higher than that in the non-trapped state, confirming the effectiveness of the single-beam optical trap in improving the SERS detection capability of the photofluidic system[133]. Furthermore, the Raman spectra of crystal violet and the pesticide thiram were successfully detected at concentrations as low as 10^{-9} mol/L and 10^{-5} mol/L, respectively, further validating the role of the single-beam optical trap in enhancing the molecular fingerprinting capability of SERS-based photofluidic chips. This integration is expected to advance highly integrated technologies and significantly enhance the overall performance and portability of optoelectronic sensing systems.

In conclusion, the integration of enrichment strategies with SERS fundamentally transforms detection capabilities by addressing the core limitation of analyte-substrate affinity. Chemical, physical, and macroscopic force field techniques synergistically enhance sensitivity through: 1) Spatial co-localization: concentrating target molecules within plasmonic hotspots, maximizing electromagnetic field interactions. 2) Signal amplification: increasing local analyte density by orders of magnitude (up to 10^4 fold), enabling attomolar detection. 3) Noise reduction: selectively isolating analytes from complex matrices (e.g., biological fluids, environmental samples), reducing background interference. 4) Versatility expansion: facilitating detection of non-adsorptive molecules (gases, ions, volatile organics) previously inaccessible to conventional SERS. This synergy transcends the limitations of hotspot engineering alone, transforming SERS from a passive substrate-dependent technique into an active sensing platform where analyte manipulation is as critical as plasmonic design. The combined approach unlocks unprecedented sensitivity, reproducibility, and real-world applicability across diverse fields.

Finally, a thorough comparison and generalization of the enrichment methods previously mentioned is presented (Table 1). This synthesis encompasses three primary strategies: chemical enrichment, which leverages specific interactions like covalent bonding or bioaffinity for selective analyte capture; physical enrichment, utilizing substrate morphology (cavities, porous structures) or wettability properties to passively or actively concentrate analytes near hotspots; and macroscopic force field enrichment, employing external fields (magnetic, acoustic, optical) to actively manipulate analytes or hotspots for

efficient localization. The comparison in Table 1 is done to assist readers and researchers in identifying the most suitable strategy for their specific applications—considering factors like analyte type, sample matrix, required sensitivity, and operational complexity, ultimately facilitating informed and efficient decision-making in method implementation. Collectively, these strategies significantly enhance SERS sensitivity and broaden its applicability by overcoming the core limitation of analyte-substrate affinity.

Summary and outlook

In this review, we start by addressing the general issues that have persisted in the development of SERS to date, focusing on solutions beyond hotspot engineering, specifically enrichment strategy. We examine the feasibility of this strategy and categorize current enrichment methods into three types based on their principles: 1) Chemical enrichment strategies. 2) Physical enrichment strategies. 3) Macroscopic force field enrichment strategies. Alongside relevant work, we discuss the advantages and disadvantages of these three categories of enrichment methods and propose optimization approaches. Looking forward, the development and promotion of SERS enrichment platforms still face several challenges: 1) Most existing enrichment platforms fail to achieve lossless enrichment, leading to insufficient detection capabilities and sample wastage. Improving current strategies or creating new lossless enrichment platforms will be a long-term research topic. 2) Nearly all SERS enrichment strategies suffer from inadequate quantitative detection capabilities, primarily due to uneven distribution of hotspot intensities within the analyte enrichment area (less than 1% of molecules located in the strongest hotspots contribute about 70% of the entire SERS intensity). Therefore, balancing hotspot strength with the enrichment working area is a necessary step toward achieving quantitative SERS detection[134]. 3) Introducing these enrichment platforms into real-world applications remains challenging, as they need to overcome complex sources of interference such as temperature, humidity, pH levels, and media. Additionally, combining micro- and nano-fabrication processes to produce stable sensors and integrating SERS enrichment platforms into practical application processes require substantial further work.

Fortunately, facing up with the intertwining influential factors and explosive data size, artificial intelligence (AI) has provided viable solutions to the above problems at SERS, presenting elite efficiency in accelerating systematic optimization and deepening understanding about the fundamental physics and spectral data, which far transcends human labors and conventional computations[135–138]. For instance, AI could aid in preparation of nanostructures: Pre-trained AI models can quantita tively establish complex high-dimensional correlations between these components. This enables inverse design methods of the desired plasmonic response to avoid the trial-and-error approach of conventional workflows, reducing both the time and cost associated with SERS nanostructure preparation. Additionally, AI-assisted guiding can predict novel SERS nanostructures that would not have been otherwise explored. The consistency of SERS nanostructures can also be improved by utilizing AI-guided automated manufacturing, such as robotic AI-chemist systems[139,140]. For quantification, by incorporating Raman signal intensity, coffee ring diameter, and POD as combined features, a machine learning-based mapping between nanoplastic concentration and coffee ring characteristics has been established[141], allowing precise predictions of dispersion concentration. The mean squared error of these predictions is remarkably low, ranging from 0.21 to 0.54, representing a 19 fold improvement in accuracy compared to traditional linear regression-based methods. This strategy effectively integrates SERS with wettability modification techniques, ensuring high sensitivity and fingerprinting capabilities, while addressing the limitations of Raman signal intensity in accurately reflecting concentration changes at ultra-low levels. To combat environmental interference, AI is further used to assist and optimize the signal acquisition process, it includes instrument adjustment, acquisition parameters and enhanced signals or images. For instance, combining image recognition algorithms with automated instrument control and feedback can efficiently locate nanostructures of interest, perform data acquisition, and obtain high-throughput standardized experimental data[142], thereby reducing fluctuations in SERS spectra. In summary, AI has been demonstrated to revolutionise SERS workflows by enabling rapid, cost-effective nanostructure design, significantly improving quantification accuracy, and automating signal acquisition. However, the effectiveness of this technology remains inherently tied to the quality of the training data and the computational resources available.

In conclusion, introducing the concept of enrichment

into SERS detection not only significantly enhances detection sensitivity but also broadens its functionality, making it an extremely attractive and promising strategy. By integrating the latest advancements and advantages from various disciplines, we have reason to believe that this diverse research approach will experience rapid de-

Table 1 | A comparative table for enrichment strategies in SERS.

Enrichment strategy category	Subtype/specific technique	Detection limit	Application scenario	Core requirements	Advantages	Disadvantages
Chemical enrichment	Direct chemical enrichment	PAEs: fmol level[74]; miRNA: fmol level[75]; L-cysteine: 0.01 μM; 2,4-dichlorophenoxyacetic acid: 0.01 ng/ml	Liquid pollutants (PAEs), biomolecules (miRNA), multiplex analysis (flavor molecules), Pesticide residues (2,4-dichlorophenoxyacetic acid)	Target molecules must bind specifically to functional groups on substrate	High selectivity; Suitable for complex matrices; Enables high-throughput platforms; Direct molecular fingerprinting	Nonspecific binding (false positives); Functional group instability; Byproduct interference; Complex modification process
	Indirect chemical enrichment	H_2S: 0.1 mmol/L[77]; Cl^-: pM level[109]	Gases (H_2S), ions (Cl^-/Cu^{2+}), pathogens (bacteria/viruses)	Requires raman tags with signal response to analyte binding	Detects raman-inactive molecules; Significant signal changes; Ideal for biosensing	Tag detachment risk; Complex labeling steps; Reporter signals may mask analyte information
Physical enrichment	Structure-based-cavity	Hg^{2+}/nanoplastics: nM level[86] H_2S (liquid): 10^{-10} M; thiram: 10^{-11} M	Liquid pollutants (ions/nanoplastics/H_2S/thiram)	Passive: Relies on diffusion; Active: Requires capillary/acousto-fluidic drive	Label-free; Uniform hotspot distribution; Wearable integration; Large surface area	Low passive efficiency; Limited to liquids; Poor gas detection; Reproducibility issues
	Structure-based-MOF/porous cages	MDA: 9.38×10^{-9} M[85]; VOCs: N/A[88]	Gas molecules (VOCs), biomarkers (tear MDA)	High surface area materials (ZIF-8/LDH); Cavity structures for gas	High adsorption capacity; Size-selective sieving; In-situ reaction monitoring	Pore blockage; Complex synthesis; Poor reusability; High cost
	Wettability-superhydrophobic	R6G: 10^{-14} M[82]	Aqueous analytes	Contact angle >150°; Controlled evaporation	High enrichment ($10^4\times$); Simple operation; Ultra-trace liquid analysis	Water-phase only; Organic solvents incompatible; Coffee-ring effect affects quantification
	Wettability-superoleophobic/SLIPS	R6G: 1 aM[122]; Sudan I: 0.1 fmol[84]	Aqueous/organic phase toxins	Fluorinated surfaces; Matching lubricant for SLIPS	Anti-solvent spreading; Multiphasic compatibility; Anti-fouling	Lubricant interference; Ineffective for gases; Complex fabrication
Macroscopic force fields	Field-assisted-magnetic	H_3N_2 virus: 10^2 $TCID_{50}$/mL[102]	Pathogens, biomolecules	Magnetic nanocomposites; External magnetic field	Rapid enrichment (minutes); Simplified sample prep; Customizable "moving hotspots"	Equipment-dependent; Low small-molecule capture; Magnetic materials may affect SERS signals
	Field-assisted-acoustic	COVID-19 DNA: 6.15×10^{-13} M[98]	Nucleic acids, biomarkers	Ultrasound-induced nanoparticle aggregation	PCR-free; <5 min detection; Nanoliter sample volume	Specialized acoustofluidic chips; Sample complexity affects aggregation; Potential biomolecular damage
	Direct enrichment-acoustic levitation	General molecules: 10^{-18} M[95]	Gas/liquid/solid phase analytes	Acoustic radiation field; Volatile solvents	Non-destructive and lossless enrichment; Universal for multiphase detection; Substrate-free	Bulky equipment; Aerosol instability; Quantification challenges; Skilled operation required

Table 1 (Continued)

Enrichment strategy category	Subtype/specific technique	Detection limit	Application scenario	Core requirements	Advantages	Disadvantages
	Direct enrichment-magnetic levitation	Microplastics: Density separation[99]	Microplastics, plasma components	Paramagnetic media ($GdCl_3$/$MnCl_2$); Strong gradient field	Non-destructive sorting; Density/size separation; Microfluidics-compatible	Size limit (>2 μm); Requires fiber-optic SERS probes; Low sensitivity; Time-consuming (hours)
Emerging technologies	Optical tweezers	CV: 10^{-9} M; Thiram: 10^{-5} M[133]	Single molecules/nanoparticles in liquids	Laser trapping of hotspots and molecules	Single-molecule sensitivity; Real-time manipulation; High spatial resolution	Expensive equipment; Low throughput; Transparent media only; Thermal damage risk
AI-optimized strategies	Inverse design/automation	Nanoplastics: MSE 0.21-0.54[141]	Universal	Big data training; Robotic automation systems	Eliminates trial-and-error; Enhanced quantification; Environmental interference suppression; Full-process optimization	Data quality-dependent; High computational load; High initial development cost

velopment, leading to significant breakthroughs in designing the next-generation hybrid SERS enrichment platforms. Achieving multifunctional SERS sensors is not only crucial for fundamental research at the molecular level but will also greatly promote practical applications in fields such as synthetic chemistry, disease diagnosis, environmental protection, and life sciences.

References

1. Deng BG, Zhang YQ, Qiu GY et al. NIR-II surface-enhanced Raman scattering nanoprobes in biomedicine: current impact and future directions. *Small* **20**, 2402235 (2024).
2. Willets KA. Super-resolution surface-enhanced Raman scattering: perspectives on the past, present, and future. *ACS Nano* **18**, 27824–27832 (2024).
3. Jin J, Guo ZN, Fan DY et al. Spotting the driving forces for SERS of two-dimensional nanomaterials. *Mater Horiz* **10**, 1087–1104 (2023).
4. Tang X, Hao Q, Hou XY et al. Exploring and engineering 2D transition metal dichalcogenides toward ultimate SERS performance. *Adv Mater* **36**, 2312348 (2024).
5. Stefancu A, Aizpurua J, Alessandri I et al. Impact of surface enhanced Raman spectroscopy in catalysis. *ACS Nano* **18**, 29337–29379 (2024).
6. Kneipp J, Kneipp K. Surface enhanced nonlinear Raman processes for advanced vibrational probing. *ACS Nano* **18**, 20851–20860 (2024).
7. Chandran A, Camden JP. Exploring excited state landscapes with surface enhanced hyper-Raman spectroscopy. *ACS Nano* **18**, 20827–20834 (2024).
8. Wustholz KL, Svoboda SA, Martin MG et al. Uncovering art's vanishing hues with surface-enhanced Raman scattering: drawing inspiration from the past for the future. *ACS Nano* **18**, 17369–17377 (2024).
9. Ma H, Pan SQ, Wang WL et al. Surface-enhanced Raman spectroscopy: current understanding, challenges, and opportunities. *ACS Nano* **18**, 14000–14019 (2024).
10. Le Ru EC, Auguié B. Enhancement factors: a central concept during 50 years of surface-enhanced Raman spectroscopy. *ACS Nano* **18**, 9773–9783 (2024).
11. Choi N, Schlücker S. Convergence of surface-enhanced Raman scattering with molecular diagnostics: a perspective on future directions. *ACS Nano* **18**, 5998–6007 (2024).
12. Logan N, Cao CN, Freitag S et al. Advancing mycotoxin detection in food and feed: novel insights from surface-enhanced Raman spectroscopy (SERS). *Adv Mater* **36**, 2309625 (2024).
13. Yu J, Yang H, Wu JG et al. Ultrafast laser fabrication of surface-enhanced Raman scattering sensors. *Opto-Electron Eng* **50**, 220333 (2023).
14. Langer J, Jimenez de Aberasturi D, Aizpurua J et al. Present and future of surface-enhanced Raman scattering. *ACS Nano* **14**, 28–117 (2020).
15. Chen RP, Li S, Ren SY et al. Micro-/nanostructures for surface-enhanced Raman spectroscopy: recent advances and perspectives. *Adv Colloid Interface Sci* **331**, 103235 (2024).
16. Zhao YP, Kumar A, Yang YJ. Unveiling practical considerations for reliable and standardized SERS measurements: lessons from a comprehensive review of oblique angle deposition-fabricated silver nanorod array substrates. *Chem Soc Rev* **53**, 1004–1057 (2024).
17. Yi J, You EM, Hu R et al. Surface-enhanced Raman spectroscopy: a half-century historical perspective. *Chem Soc Rev* **54**, 1453–1551 (2025).
18. Chaudhry I, Hu GH, Ye HP et al. Toward modeling the complexity of the chemical mechanism in SERS. *ACS Nano* **18**, 20835–20850 (2024).
19. Tan JB, Du BQ, Ji C et al. Thermoelectric field-assisted Raman scattering and photocatalysis with GaN-plasmonic metal composites. *ACS Photonics* **10**, 2216–2225 (2023).
20. Ji C, Lu JX, Shan BJ et al. The origin of Mo_2C films for surface-enhanced Raman scattering analysis: electromagnetic or chemical enhancement. *J Phys Chem Lett* **13**, 8864–8871 (2022).

21. Li CH, Xu SC, Yu J et al. Local hot charge density regulation: vibration-free pyroelectric nanogenerator for effectively enhancing catalysis and in-situ surface enhanced Raman scattering monitoring. *Nano Energy* **81**, 105585 (2021).
22. Shao MR, Ji C, Tan JB et al. Ferroelectrically modulate the Fermi level of graphene oxide to enhance SERS response. *Opto-Electron Adv* **6**, 230094 (2023).
23. Wu Y, Sun TY, Shao MR et al. Pyroelectrically driven charge transfer and its advantages on SERS and self-cleaning property. *Laser Photonics Rev* **19**, 2401152 (2025).
24. Liu BW, Yao X, Chen S et al. Large-area hybrid plasmonic optical cavity (HPOC) substrates for surface-enhanced Raman spectroscopy. *Adv Funct Mater* **28**, 1802263 (2018).
25. Barveen NR, Wang TJ, Chang YH. Photochemical synthesis of Au nanostars on PMMA films by ethanol action as flexible SERS substrates for in-situ detection of antibiotics on curved surfaces. *Chem Eng J* **431**, 134240 (2022).
26. Han XM, Koh CSL, Lee HK et al. Microchemical plant in a liquid droplet: plasmonic liquid marble for sequential reactions and attomole detection of toxin at microliter scale. *ACS Appl Mater Interfaces* **9**, 39635–39640 (2017).
27. Xie LP, Zeng HDL, Zhu JX et al. State of the art in flexible SERS sensors toward label-free and onsite detection: from design to applications. *Nano Res* **15**, 4374–4394 (2022).
28. Usha SP, Manoharan H, Deshmukh R et al. Attomolar analyte sensing techniques (AttoSens): a review on a decade of progress on chemical and biosensing nanoplatforms. *Chem Soc Rev* **50**, 13012–13089 (2021).
29. Li QQ, Huo HQ, Wu Y et al. Design and synthesis of SERS materials for in vivo molecular imaging and biosensing. *Adv Sci (Weinh)* **10**, 2202051 (2023).
30. Allakhverdiev ES, Khabatova VV, Kossalbayev BD et al. Raman spectroscopy and its modifications applied to biological and medical research. *Cells* **11**, 386 (2022).
31. Plou J, Valera PS, García I et al. Prospects of surface-enhanced Raman spectroscopy for biomarker monitoring toward precision medicine. *ACS Photonics* **9**, 333–350 (2022).
32. Luo ZW, Chen HR, Bi XY et al. Monitoring kinetic processes of drugs and metabolites: surface-enhanced Raman spectroscopy. *Adv Drug Deliv Rev* **217**, 115483 (2025).
33. Bi XY, Qian XH, Xue BS et al. Molecule-resolvable SERSome for metabolic profiling. *Chem* (2025). https://doi.org/10.1016/j.chempr.2025.102528
34. Xie YS, Huang JQ, Yang M et al. Nucleic acid-mediated SERS biosensors: signal enhancement strategies and applications. *Biosens Bioelectron* **282**, 117519 (2025).
35. Kant K, Beeram R, Cao Y et al. Plasmonic nanoparticle sensors: current progress, challenges, and future prospects. *Nanoscale Horiz* **9**, 2085–2166 (2024).
36. Allegretto JA, Dostalek J. Metal-organic frameworks in surface enhanced Raman spectroscopy-based analysis of volatile organic compounds. *Adv Sci (Weinh)* **11**, 2401437 (2024).
37. Lu YY, Yang XW, Bao HM et al. Vortex engineering on oxide bowl-coated oxide/gold dual-layer array for dual electrical/spectroscopic monitoring of volatile organic compounds. *Adv Funct Mater* **34**, 2402173 (2024).
38. Fu JH, Zhong Z, Xie D et al. SERS-active MIL-100(Fe) sensory array for ultrasensitive and multiplex detection of VOCs. *Angew Chem Int Ed* **59**, 20489–20498 (2020).
39. Zhou X, Hu ZW, Yang DT et al. Bacteria detection: from powerful SERS to its advanced compatible techniques. *Adv Sci (Weinh)* **7**, 2001739 (2020).
40. Porter MD, Lipert RJ, Siperko LM et al. SERS as a bioassay platform: fundamentals, design, and applications. *Chem Soc Rev* **37**, 1001–1011 (2008).
41. Rutter JW, Dekker L, Clare C et al. A bacteriocin expression platform for targeting pathogenic bacterial species. *Nat Commun* **15**, 6332 (2024).
42. Song LP, Chen J, Xu BB et al. Flexible plasmonic biosensors for healthcare monitoring: progress and prospects. *ACS Nano* **15**, 18822–18847 (2021).
43. Hasan MAM, Qian WQ, Wang JB et al. Eco-friendly and low-cost heavy metal ion detection via droplet-generated triboelectricity. *Nano Energy* **131**, 110320 (2024).
44. Moon T, Joo H, Das B et al. Adaptive gap-tunable surface-enhanced Raman spectroscopy. *Nano Lett* **24**, 3777–3784 (2024).
45. Jeon TY, Park SG, Kim DH et al. Standing-wave-assisted creation of nanopillar arrays with vertically integrated nanogaps for SERS-active substrates. *Adv Funct Mater* **25**, 4681–4688 (2015).
46. Li JF, Xie QH, Li JB et al. Macroscale TiO_2 microspherical arrays with multiple synergistic effect for highly sensitive surface-enhanced Raman scattering. *Adv Funct Mater* **34**, 2400523 (2024).
47. Gao TX, Yachi T, Shi X et al. Ultrasensitive surface-enhanced Raman scattering platform for protein detection via active delivery to nanogaps as a hotspot. *ACS Nano* **18**, 21593–21606 (2024).
48. Shvalya V, Filipič G, Zavašnik J et al. Surface-enhanced Raman spectroscopy for chemical and biological sensing using nanoplasmonics: the relevance of interparticle spacing and surface morphology. *Appl Phys Rev* **7**, 031307 (2020).
49. Tian Y, Wu FX, Lv XL et al. Enantioselective surface-enhanced Raman scattering by chiral Au nanocrystals with finely modulated chiral fields and internal standards. *Adv Mater* **36**, 2403373 (2024).
50. Ding SY, You EM, Tian ZQ et al. Electromagnetic theories of surface-enhanced Raman spectroscopy. *Chem Soc Rev* **46**, 4042–4076 (2017).
51. Yan S, Ma H, Bao YF et al. Optical responses of metallic plasmonic arrays under the localized excitation. *Nano Res* **17**, 1571–1577 (2024).
52. Zhang C, Li CH, Yu J et al. SERS activated platform with three-dimensional hot spots and tunable nanometer gap. *Sens Actuators B Chem* **258**, 163–171 (2018).
53. Li CH, Zhang C, Xu SC et al. Experimental and theoretical investigation for a hierarchical SERS activated platform with 3D dense hot spots. *Sens Actuators B Chem* **263**, 408–416 (2018).
54. Chen MP, Liu D, Du XY et al. 2D materials: excellent substrates for surface-enhanced Raman scattering (SERS) in chemical sensing and biosensing. *Trends Analyt Chem* **130**, 115983 (2020).
55. Yang W, Lim DK. Recent advances in the synthesis of intra-nanogap Au plasmonic nanostructures for bioanalytical applications. *Adv Mater* **32**, 2002219 (2020).
56. Sriram P, Manikandan A, Chuang FC et al. Hybridizing plasmonic materials with 2D-transition metal dichalcogenides toward functional applications. *Small* **16**, 1904271 (2020).

57. Guselnikova O, Lim H, Kim HJ et al. New trends in nanoarchitectured SERS substrates: nanospaces, 2D materials, and organic heterostructures. *Small* **18**, 2107182 (2022).
58. Liu YW, Ma H, Han XX et al. Metal-semiconductor heterostructures for surface-enhanced Raman scattering: synergistic contribution of plasmons and charge transfer. *Mater Horiz* **8**, 370–382 (2021).
59. Lu ZY, Liu YJ, Wang MH et al. A novel natural surface-enhanced Raman spectroscopy (SERS) substrate based on graphene oxide-Ag nanoparticles-mytilus coruscus hybrid system. *Sens Actuators B Chem* **261**, 1–10 (2018).
60. Zhang C, Li Z, Jiang SZ et al. U-bent fiber optic SPR sensor based on graphene/AgNPs. *Sens Actuators B Chem* **251**, 127–133 (2017).
61. Yang MR, Pan YY, Ji C et al. Three-dimensional MXene-Ag-NP hollow spheres for in situ surface-enhanced Raman scattering detection of catalysis reactions. *J Phys Chem Lett* **14**, 9019–9026 (2023).
62. Bharati MSS, Soma VR. Flexible SERS substrates for hazardous materials detection: recent advances. *Opto-Electron Adv* **4**, 210048 (2021).
63. Koya AN, Zhu XC, Ohannesian N et al. Nanoporous metals: from plasmonic properties to applications in enhanced spectroscopy and photocatalysis. *ACS Nano* **15**, 6038–6060 (2021).
64. Lee HK, Lee YH, Koh CSL et al. Designing surface-enhanced Raman scattering (SERS) platforms beyond hotspot engineering: emerging opportunities in analyte manipulations and hybrid materials. *Chem Soc Rev* **48**, 731–756 (2019).
65. Li JY, Heng H, Lv JL et al. Graphene oxide-assisted and DNA-modulated SERS of AuCu alloy for the fabrication of apurinic/apyrimidinic endonuclease 1 biosensor. *Small* **15**, 1901506 (2019).
66. Xu SC, Jiang SZ, Wang JH et al. Graphene isolated Au nanoparticle arrays with high reproducibility for high-performance surface-enhanced Raman scattering. *Sens Actuators B Chem* **222**, 1175–1183 (2016).
67. Lee S, Hahm MG, Vajtai R et al. Utilizing 3D SERS active volumes in aligned carbon nanotube scaffold substrates. *Adv Mater* **24**, 5261–5266 (2012).
68. Qiu BC, Xing MY, Yi QY et al. Chiral carbonaceous nanotubes modified with titania nanocrystals: plasmon-free and recyclable SERS sensitivity. *Angew Chem Int Ed* **54**, 10643–10647 (2015).
69. Dawson P, Duenas JA, Boyle MG et al. Combined antenna and localized plasmon resonance in Raman scattering from random arrays of silver-coated, vertically aligned multiwalled carbon nanotubes. *Nano Lett* **11**, 365–371 (2011).
70. Niu JJ, Schrlau MG, Friedman G et al. Carbon nanotube-tipped endoscope for in situ intracellular surface-enhanced Raman spectroscopy. *Small* **7**, 540–545 (2011).
71. Cheng HH, Zhao Y, Fan YQ et al. Graphene-quantum-dot assembled nanotubes: a new platform for efficient Raman enhancement. *ACS Nano* **6**, 2237–2244 (2012).
72. Li H, Xu Q, Wang XZ et al. Ultrasensitive surface-enhanced Raman spectroscopy detection based on amorphous molybdenum oxide quantum dots. *Small* **14**, 1801523 (2018).
73. Liu DH, Chen XS, Hu YB et al. Raman enhancement on ultra-clean graphene quantum dots produced by quasi-equilibrium plasma-enhanced chemical vapor deposition. *Nat Commun* **9**, 193 (2018).
74. Yang YY, Li YT, Li XJ et al. Controllable *in situ* fabrication of portable AuNP/mussel-inspired polydopamine molecularly imprinted SERS substrate for selective enrichment and recognition of phthalate plasticizers. *Chem Eng J* **402**, 125179 (2020).
75. Lu XH, Hu C, Jia DL et al. Amplification-free and mix-and-read analysis of multiplexed MicroRNAs on a single plasmonic microbead. *Nano Lett* **21**, 6718–6724 (2021).
76. Li JX, Shen WZ, Liang XY et al. 2D film-like magnetic SERS tag with enhanced capture and detection abilities for immunochromatographic diagnosis of multiple bacteria. *Small* **20**, 2310014 (2024).
77. Li DW, Qu LL, Hu K et al. Monitoring of endogenous hydrogen sulfide in living cells using surface-enhanced Raman scattering. *Angew Chem Int Ed* **54**, 12758–12761 (2015).
78. Leong YX, Lee YH, Koh CSL et al. Surface-enhanced Raman scattering (SERS) taster: a machine-learning-driven multireceptor platform for multiplex profiling of wine flavors. *Nano Lett* **21**, 2642–2649 (2021).
79. Zhang SH, Mei YX, Liu JQ et al. Alkyne-tagged SERS nanoprobe for understanding Cu^{+} and Cu^{2+} conversion in cuproptosis processes. *Nat Commun* **15**, 3246 (2024).
80. Xu BB, Zhang YL, Zhang WY et al. Silver-coated rose petal: green, facile, low-cost and sustainable fabrication of a SERS substrate with unique superhydrophobicity and high efficiency. *Adv Opt Mater* **1**, 56–60 (2013).
81. Wong TS, Kang SH, Tang SKY et al. Bioinspired self-repairing slippery surfaces with pressure-stable omniphobicity. *Nature* **477**, 443–447 (2011).
82. Song J, Cheng WF, Nie MT et al. Partial leidenfrost evaporation-assisted ultrasensitive surface-enhanced Raman spectroscopy in a Janus water droplet on hierarchical plasmonic micro-/nanostructures. *ACS Nano* **14**, 9521–9531 (2020).
83. Qiao XZ, Chen XY, Huang CH et al. Detection of exhaled volatile organic compounds improved by hollow nanocages of layered double hydroxide on Ag nanowires. *Angew Chem Int Ed* **58**, 16523–16527 (2019).
84. Li X, Lee HK, Phang IY et al. Superhydrophobic-oleophobic Ag nanowire platform: an analyte-concentrating and quantitative aqueous and organic toxin surface-enhanced Raman scattering sensor. *Anal Chem* **86**, 10437–10444 (2014).
85. Li JM, Yu HZ, Zhao JM et al. Metal-organic framework-based surface-enhanced Raman scattering sensing platform for trace malondialdehyde detection in tears. *Nano Lett* **24**, 7792–7799 (2024).
86. Li J, Liu H, Chen SY et al. Particle-in-molybdenum disulfide-coated cavity structure with a Raman internal standard for sensitive Raman detection of water contaminants from ions to <300 nm nanoplastics. *J Phys Chem Lett* **13**, 5815–5823 (2022).
87. Li HZ, Yang Q, Hou J et al. Bioinspired micropatterned superhydrophilic Au-areoles for surface-enhanced Raman scattering (SERS) trace detection. *Adv Funct Mater* **28**, 1800448 (2018).
88. Li AL, Qiao XZ, Liu KY et al. Hollow metal organic framework improves the sensitivity and anti-interference of the detection of exhaled volatile organic compounds. *Adv Funct Mater* **32**, 2202805 (2022).
89. Lee HK, Lee YH, Morabito JV et al. Driving CO_2 to a quasi-condensed phase at the interface between a nanoparticle sur-

face and a metal-organic framework at 1 bar and 298 K. *J Am Chem Soc* **139**, 11513–11518 (2017).
90. He XC, Yang SJ, Xu TL et al. Microdroplet-captured tapes for rapid sampling and SERS detection of food contaminants. *Biosens Bioelectron* **152**, 112013 (2020).
91. Hao NJ, Liu PZ, Bachman H et al. Acoustofluidics-assisted engineering of multifunctional three-dimensional zinc oxide nanoarrays. *ACS Nano* **14**, 6150–6163 (2020).
92. Ding QQ, Wang J, Chen XY et al. Quantitative and sensitive SERS platform with analyte enrichment and filtration function. *Nano Lett* **20**, 7304–7312 (2020).
93. De Angelis F, Gentile F, Mecarini F et al. Breaking the diffusion limit with super-hydrophobic delivery of molecules to plasmonic nanofocusing SERS structures. *Nat Photonics* **5**, 682–687 (2011).
94. Baday M, Calamak S, Durmus NG et al. Integrating cell phone imaging with magnetic levitation (i-LEV) for label-free blood analysis at the point-of-living. *Small* **12**, 1222–1229 (2016).
95. Chen XY, Ding QQ, Bi C et al. Lossless enrichment of trace analytes in levitating droplets for multiphase and multiplex detection. *Nat Commun* **13**, 7807 (2022).
96. Fan XC, Hao Q, Li MZ et al. Hotspots on the move: active molecular enrichment by hierarchically structured micromotors for ultrasensitive SERS sensing. *ACS Appl Mater Interfaces* **12**, 28783–28791 (2020).
97. Ge SC, Nemiroski A, Mirica KA et al. Magnetic levitation in chemistry, materials science, and biochemistry. *Angew Chem Int Ed* **59**, 17810–17855 (2020).
98. Luo Y, Zhou MY, Fan C et al. Active enrichment of nanoparticles for ultra-trace point-of-care COVID-19 detection. *Anal Chem* **95**, 5316–5322 (2023).
99. Ren XP, Breadmore MC, Maya F. Biphasic magnetic levitation to detect organic pollutants on microplastics. *Anal Chem* **94**, 9033–9039 (2022).
100. Ren XP, Breadmore MC, Maya F. Bidimensional dynamic magnetic levitation: sequential separation of microplastics by density and size. *Anal Chem* **96**, 3259–3266 (2024).
101. Winkleman A, Perez-Castillejos R, Gudiksen KL et al. Density-based diamagnetic separation: devices for detecting binding events and for collecting unlabeled diamagnetic particles in paramagnetic solutions. *Anal Chem* **79**, 6542–6550 (2007).
102. Yin BH, Ho WKH, Zhang Q et al. Magnetic-responsive surface-enhanced Raman scattering platform with tunable hot spot for ultrasensitive virus nucleic acid detection. *ACS Appl Mater Interfaces* **14**, 4714–4724 (2022).
103. Moncal KK, Yaman S, Durmus NG. Levitational 3D bioassembly and density-based spatial coding of levitoids. *Adv Funct Mater* **32**, 2204092 (2022).
104. Pakpour S, Vojnits K, Alousi S et al. Magnetic levitation system isolates and purifies airborne viruses. *ACS Nano* **17**, 13393–13407 (2023).
105. Leong SX, Tan E, Han X et al. Surface-enhanced Raman scattering-based surface chemotaxonomy: combining bacteria extracellular matrices and machine learning for rapid and universal species identification. *ACS Nano* **17**, 23132–23143 (2023).
106. Kao YC, Han XM, Lee YH et al. Multiplex surface-enhanced Raman scattering identification and quantification of urine metabolites in patient samples within 30 min. *ACS Nano* **14**, 2542–2552 (2020).
107. Tan EX, Leong SX, Liew WA et al. Forward-predictive SERS-based chemical taxonomy for untargeted structural elucidation of epimeric cerebrosides. *Nat Commun* **15**, 2582 (2024).
108. Qu C, Fang H, Yu FF et al. Artificial nose of scalable plasmonic array gas sensor for multi-dimensional SERS recognition of volatile organic compounds. *Chem Eng J* **482**, 148773 (2024).
109. Tsoutsi D, Montenegro JM, Dommershausen F et al. Quantitative surface-enhanced Raman scattering ultradetection of atomic inorganic ions: the case of chloride. *ACS Nano* **5**, 7539–7546 (2011).
110. Xiao YJ, Liu WJ, Zhang Y et al. Simple and rapid co-freezing construction of SERS signal probes for the sensitive detection of pathogens. *Chem Eng J* **466**, 143066 (2023).
111. Shi YF, Fang JX. Yolk-shell hierarchical pore Au@MOF nanostructures: efficient gas capture and enrichment for advanced breath analysis. *Nano Lett* **24**, 10139–10147 (2024).
112. Qin XJ, Xiang YH, Mao LF et al. Buoyant metal-organic framework corona-driven fast isolation and ultrasensitive profiling of circulating extracellular vesicles. *ACS Nano* **18**, 14569–14582 (2024).
113. Lu YY, Zhang X, Zhao LY et al. Metal-organic framework template-guided electrochemical lithography on substrates for SERS sensing applications. *Nat Commun* **14**, 5860 (2023).
114. Dang HJ, Joung YJ, Yang JY et al. Advancing COVID-19 diagnosis: enhancement in SERS-PCR with 30-nm Au nanoparticle-internalized nanodimpled substrates. *Small* **20**, 2403672 (2024).
115. Im H, Bantz KC, Lee SH et al. Self-assembled plasmonic nanoring cavity arrays for SERS and LSPR biosensing. *Adv Mater* **25**, 2678–2685 (2013).
116. Feng L, Ma RP, Wang YD et al. Silver-coated elevated bowtie nanoantenna arrays: improving the near-field enhancement of gap cavities for highly active surface-enhanced Raman scattering. *Nano Res* **8**, 3715–3724 (2015).
117. Hosono N, Uemura T. Metal-organic frameworks for macromolecular recognition and separation. *Matter* **3**, 652–663 (2020).
118. Pei ZY, Li J, Ji C et al. Flexible Cascaded wire-in-cavity-in-bowl structure for high-performance and polydirectional sensing of contaminants in microdroplets. *J Phys Chem Lett* **14**, 5932–5939 (2023).
119. Huang CH, Li AL, Chen XY et al. Understanding the role of metal-organic frameworks in surface-enhanced Raman scattering application. *Small* **16**, 2004802 (2020).
120. Qureshi WA, Haider SNUZ, Qaiser MA et al. Breakthrough in plasmonic enhanced MOFs: design, synthesis, and catalytic mechanisms for various photocatalytic applications. *Environ Res* **277**, 121257 (2025).
121. Yuan YT, Mi JJ, Wang M et al. The preparation and surface enhanced Raman scattering spectroscopy of AuNRs@ZIF-8. *Opto-Electron Eng* **50**, 230029 (2023).
122. Yang SK, Dai XM, Stogin BB et al. Ultrasensitive surface-enhanced Raman scattering detection in common fluids. *Proc Natl Acad Sci USA* **113**, 268–273 (2016).
123. Mao ZM, Li P, Wu MX et al. Enriching nanoparticles *via* acoustofluidics. *ACS Nano* **11**, 603–612 (2017).
124. Leopold N, Haberkorn M, Laurell T et al. On-line monitoring of airborne chemistry in levitated nanodroplets: in situ synthesis and application of SERS-active Ag-sols for trace analysis by FT-Raman spectroscopy. *Anal Chem* **75**, 2166–2171 (2003).
125. Santesson S, Johansson J, Taylor LS et al. Airborne chem-

istry coupled to Raman spectroscopy. *Anal Chem* **75**, 2177–2180 (2003).
126. Gu YY, Chen CY, Rufo J et al. Acoustofluidic holography for micro- to nanoscale particle manipulation. *ACS Nano* **14**, 14635–14645 (2020).
127. Hao NJ, Pei ZC, Liu PZ et al. Acoustofluidics-assisted fluorescence-SERS bimodal biosensors. *Small* **16**, 2005179 (2020).
128. Kitazawa K, Ikezoe Y, Uetake H et al. Magnetic field effects on water, air and powders. *Phys B Condens Matter* **294–295**, 709–714 (2001).
129. Ashkarran AA, Gharibi H, Zeki DA et al. Multi-omics analysis of magnetically levitated plasma biomolecules. *Biosens Bioelectron* **220**, 114862 (2023).
130. Sneh T, Corsetti S, Notaros M et al. Optical tweezing of microparticles and cells using silicon-photonics-based optical phased arrays. *Nat Commun* **15**, 8493 (2024).
131. Svedberg F, Li ZP, Xu HX et al. Creating hot nanoparticle pairs for surface-enhanced Raman spectroscopy through optical manipulation. *Nano Lett* **6**, 2639–2641 (2006).
132. Pesce G, Jones PH, Maragò OM et al. Optical tweezers: theory and practice. *Eur Phys J Plus* **135**, 949 (2020).
133. Sun N, Gan Y, Wu YJ et al. Single-beam optical trap-based surface-enhanced Raman scattering optofluidic molecular fingerprint spectroscopy detection system. *Opto-Electron Adv* **8**, 240182 (2025).
134. Bi XY, Czajkowsky DM, Shao ZF et al. Digital colloid-enhanced Raman spectroscopy by single-molecule counting. *Nature* **628**, 771–775 (2024).
135. Bi XY, Lin L, Chen Z et al. Artificial intelligence for surface-enhanced Raman spectroscopy. *Small Methods* **8**, 2301243 (2024).
136. Yi J, You EM, Liu GK et al. AI-nano-driven surface-enhanced Raman spectroscopy for marketable technologies. *Nat Nanotechnol* **19**, 1758–1762 (2024).
137. Bi XY, Ai XY, Wu ZY et al. Artificial intelligence-powered surface-enhanced Raman spectroscopy for biomedical applications. *Anal Chem* **97**, 6826–6846 (2025).
138. Xue BS, Bi XY, Dong ZY et al. Deep spectral component filtering as a foundation model for spectral analysis demonstrated in metabolic profiling. *Nat Mach Intell* **7**, 743–757 (2025).
139. Zhu Q, Zhang F, Huang Y et al. An all-round AI-chemist with a scientific mind. *Natl Sci Rev* **9**, nwac190 (2022).
140. Burger B, Maffettone PM, Gusev VV et al. A mobile robotic chemist. *Nature* **583**, 237–241 (2020).
141. Lin XN, Lei FC, Liang X et al. Quantitative detection of trace nanoplastics (down to 50 nm) via surface-enhanced Raman scattering based on the multiplex-feature coffee ring. *Opto-Electron Adv* **8**, 240260 (2025).
142. Grys DB, de Nijs B, Huang JY et al. SERSbot: revealing the details of SERS multianalyte sensing using full automation. *ACS Sens* **6**, 4507–4514 (2021).

Acknowledgements

We are grateful for financial supports from the National Natural Science Foundation of China (12174229, 12474408), Taishan Scholars Program of Shandong Province (tsqn202306152), Qingchuang Science and Technology Plan of Shandong Province (2021KJ006), Shandong Provincial Natural Science Foundation (ZR2022YQ02).

Author contributions

This endeavor was accomplished through the collective efforts of all authors: Prof. Chao Zhang Jing Yu, and Zhen Li orchestrated and supervised the entire research endeavor; Dr. Zhiyang Pei, drafted and refined the manuscript; Dr. Mingrui Shao, Chang Ji, Yang Wu, Xiaofei Zhao and Baoyuan Man helped with review and editing.

Competing interests

The authors declare no competing financial interests.

Scan for Article PDF